Resonant light–atom interactions

9

In this chapter we shall study the processes that occur when an atom is irradiated with a light beam that is resonant with one of its natural frequencies. We shall start by making a few general observations, and then give a detailed analysis of the process based on the time-dependent Schrödinger equation. This will lead us to the concept of Rabi oscillations, from which we shall be able to obtain a deeper understanding of how absorption transitions work. In so doing we shall introduce the Bloch sphere, which will be very useful for understanding quantum gates in Chapter 13.

The subject material developed here assumes that the reader is familiar with the standard treatment of optical transitions in atoms and the Einstein coefficients. A summary of the main points may be found in Chapter 4.

9.1 Introduction

The treatment of the interaction between light and atoms was pivotal in the development of quantum theory in the first half of the twentieth century. In 1913 Bohr postulated that a quantum of light of angular frequency ω is absorbed or emitted whenever an atom jumps between two quantized energy levels E_1 and E_2 that satisfy:

$$E_2 - E_1 = \hbar\omega. \tag{9.1}$$

The theory was developed by Einstein in 1916–7 when he introduced the **Einstein coefficients** to quantify the rate at which the absorption and emission of quanta occur. In the same paper he discovered the process of stimulated emission, which later proved to be the basis of laser operation.

The picture of the interaction process between light and atoms that emerges from Bohr and Einstein's treatment is illustrated in Fig. 9.1. The absorption process is viewed in terms of the destruction of a photon from the light beam with the simultaneous excitation of the atom, while the emission process corresponds to the addition of a photon to the light field and the simultaneous de-excitation of the atom.

Consider the absorption process shown in Fig. 9.1(a). We imagine that the atom is initially in the lower level, and a light beam of angular frequency ω is turned on at time $t = 0$. At some later time the atom makes the jump to the excited state, and a photon is absorbed from the

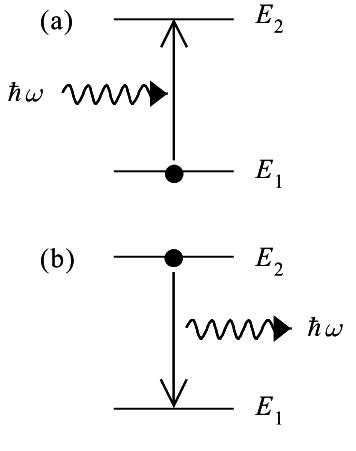

Fig. 9.1 Optical transitions between quantized energy levels: (a) absorption, and (b) spontaneous emission. Stimulated emission processes are not considered here.

light beam. Similarly, in the emission process shown in Fig. 9.1(b), the atom is in the excited state at time $t = 0$. After a time typically equal to the radiative lifetime of the excited state, a photon of angular frequency ω is emitted. Once these processes have been completed, we say that the atom has made a **transition** from level $1 \rightarrow 2$ and vice versa.

The question we wish to address in this chapter is as follows. What happens to the irradiated atom *before* the absorption transition is complete? The Einstein treatment of the process does not address this issue. To do so, we will have to solve the time-dependent Schrödinger equation for the atom with the light included. This will be the subject of Section 9.3, and its consequences will be explored in the following sections. Before we can do this, we must first clarify a few basic concepts and explain the approximations which allow us to set up the problem in a way that can be solved easily. These will be the subject of the next section.

It is, of course, equally interesting to ask about the mechanism of spontaneous emission in more detail. At the level of the Einstein approach, it is viewed as a purely random process governed by decay probabilities. At a deeper level, however, we can consider it as a stimulated emission event triggered by a vacuum photon. The randomness is then attributed to the quantum noise of the zero-point fluctuations of the electromagnetic field. (See Section 7.4.) Further discussion of this topic will be postponed to the next chapter. We shall see in Section 10.3 that the spontaneous emission rate of an atom is not an absolute quantity, but can in fact be controlled by suppressing or enhancing the density of the photon modes by situating the atom within a resonant cavity.

9.2 Preliminary concepts

9.2.1 The two-level atom approximation

The quantum treatment of the interaction between light and atoms is usually developed in terms of the **two-level atom approximation**. This approximation is applicable when the frequency of the light coincides with one of the optical transitions of the atom. The condition is specified in eqn 9.1 and is depicted schematically in Fig. 9.2. The atom will have many quantum levels, and there will be many possible optical transitions between them. However, in the two-level atom approximation we only consider the specific transition that satisfies eqn 9.1 and ignore all the other levels. It is customary to label the lower and upper levels as 1 and 2, respectively.

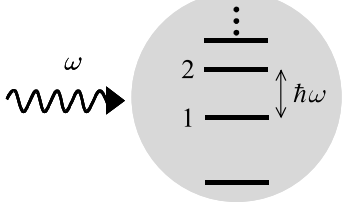

Fig. 9.2 The two-level atom approximation. When the light angular frequency ω coincides with one of the optical transitions of the atom, we have a resonant interaction between that transition and the light field. We can therefore neglect the other levels of the atom, which only weakly interact with the light because they are off-resonance.

The physical basis for the two-level approximation is the fact that we are dealing with a **resonance** phenomenon. In the classical picture of light–atom interactions, the light beam induces dipole oscillations in the atom, which then re-radiate at the same frequency. If the light frequency corresponds to the natural frequency of the atom, the magnitude of the dipole oscillations will be large and the interaction between the atom and the light will be strong. (See Exercise 9.1.) On the other hand, if the light frequency is far away from the natural frequency of the atom

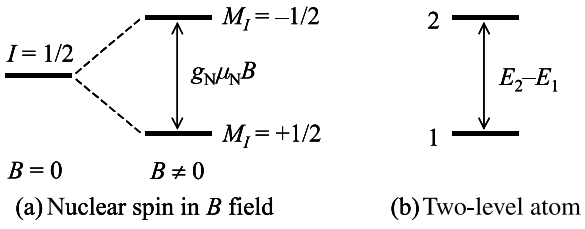

Fig. 9.3 A spin 1/2 system in a magnetic field of strength B along the z-axis (a) is formally equivalent to a two-level atom (b). For historical reasons, we usually consider nuclear spin systems rather than electronic ones, in which case the field splitting is determined by the nuclear g-factor g_N and the nuclear Bohr magneton μ_N.

(i.e. off-resonance), then the magnitude of the driven oscillations will be small, and the light–atom interaction will be small. In other words, the interaction between the light and the atom is very much stronger for the case of resonant than off-resonant transitions, and so it is a good approximation to ignore the latter.

It is obvious that the assumption that only the resonant levels matter is an approximation. In many cases, the approximation is very good. On the other hand, the presence of the off-resonant levels may become important indirectly. When the atom is in level 2, it could make transitions to other lower levels in addition to level 1. This would cause a loss of atoms from the system considered, and would effectively damp the interaction between the light and the atom. Hence the simplest way to include other levels in the analysis is to include damping terms. We shall see the importance of damping in Section 9.5.

A useful analogy can be made between the properties of two-level atoms and those of spin 1/2 particles in a magnetic field. Figure 9.3(a) shows how a magnetic field of strength B splits a spin 1/2 system into a doublet through the Zeeman effect. The Zeeman-split levels are formally equivalent to the two-level atom shown in Fig. 9.3(b). The reason for making the analogy is that the theory of the resonant interaction between microwave radiation and the Zeeman-split nuclear spin states had been developed in the 1940s to account for a whole range of nuclear magnetic resonance (NMR) phenomena. With the advent of the laser in 1960, the same types of phenomena were soon observed in two-level atomic systems at optical frequencies. We shall explore this analogy further in Section 9.6.

9.2.2 Coherent superposition states

The concept of coherent superposition states lies at the heart of quantum computation. (See Section 13.2.)

The treatment of the resonant interaction between an atom and a light field involves the concept of **coherent superposition states**. Wave function coherence gives rise to many of the phenomena that make quantum systems behave differently from classical ones. For this reason, it is important to remind ourselves of what coherent superposition states are, and how they differ from **statistical mixtures**.

Consider a quantum system with two levels, such as a two-level atom or a spin 1/2 nucleus in a magnetic field. (See Fig. 9.3.) We assume that there is some way of measuring whether the system is in the lower or upper level. For example, in the case of the two-level atom we could determine whether the atom is in the upper level by looking for spontaneous emission at angular frequency ω. Similarly, in the case of the nuclear spin we could carry out a Stern–Gerlach experiment to determine I_z. The wave function for the system may in general be written in the form:

$$|\psi\rangle = c_1|1\rangle + c_2|2\rangle, \tag{9.2}$$

where c_1 and c_2 describe the wave function amplitude coefficients for the two states of the atom or nucleus. If we make a measurement we would obtain the result appropriate to level 1 with probability $|c_1|^2$ and that for level 2 with probability $|c_2|^2$.

Now consider a gas of N_0 identical two-level particles (e.g. two-level atoms or spin 1/2 nuclei) with N_1 particles in the lower level and N_2 in the upper level. Such a gas is called a **statistical mixture**. By setting $|c_1|^2 = N_1/N_0$ and $|c_2|^2 = N_2/N_0$ we would obtain the same results as for repeated measurements on a gas of N_0 particles in the superposition state given by eqn 9.2. What, then, is the difference? The answer is that each of the particles in the superposition state is in some sense simultaneously in the $|1\rangle$ and $|2\rangle$ states, and this leads to the possibility of wave function interference. In the statistical mixture, by contrast, a given particle is *either* in level 1 *or* in level 2, and no wave function interference can occur.

A useful analogy can be made here with interference effects in light beams. This analogy also helps to explain why we often include the adjective 'coherent' in the description of the superposition states. Consider two overlapping light beams of the same frequency with phases ϕ_1 and ϕ_2 respectively. The resultant field is given by:

$$\begin{aligned}\mathcal{E} &= \mathcal{E}_1 \mathrm{e}^{-\mathrm{i}(\omega t+\phi_1)} + \mathcal{E}_2 \mathrm{e}^{-\mathrm{i}(\omega t+\phi_2)} \\ &= \mathcal{E}_1 \mathrm{e}^{-\mathrm{i}(\omega t+\phi_1)} \left(1 + (\mathcal{E}_2/\mathcal{E}_1)\mathrm{e}^{-\mathrm{i}(\phi_2-\phi_1)}\right),\end{aligned} \tag{9.3}$$

where ω is the angular frequency, and $\mathcal{E}_1$ and $\mathcal{E}_2$ are the amplitudes. The beams will interfere if they are *coherent*, that is, when

$$\Delta\phi = \phi_2 - \phi_1 = \text{constant}, \tag{9.4}$$

at a given point in space. In this case, there will be some positions where $\Delta\phi = (\text{even integer} \times \pi)$ and we have a bright fringe, and others where $\Delta\phi = (\text{odd integer} \times \pi)$ and we have a dark fringe. On the other hand, if the beams are *incoherent*, the phases vary randomly with time relative to each other, and there will be no interference. In this case the powers of the beams will just add together, so that the resultant will be given by:

$$|\mathcal{E}|^2 = |\mathcal{E}_1|^2 + |\mathcal{E}_2|^2. \tag{9.5}$$

The analogy with the two-level superposition states can be made apparent by setting $c_1 \rightarrow \mathcal{E}_1 \exp(-\mathrm{i}\phi_1)$ and $c_2 \rightarrow \mathcal{E}_2 \exp(-\mathrm{i}\phi_2)$. We then see that wave function interference can only occur when there is a definite phase relationship between c_1 and c_2. This occurs in the superposition state, but not in a statistical mixture, where the different particle wave functions all have random phases with respect to each other.

In the treatment of the light–atom interactions given in this chapter, we shall see that a light pulse links the phases of the upper and lower levels of an atom so that wave function coherence is present. This gives rise to new phenomena which are not considered in the Einstein analysis, as it only deals with statistical mixtures. In particular, we shall see that while the light pulse is present, the atom oscillates between the upper and lower levels. This rather striking conclusion appears to be at odds with our simpler picture based on discrete transitions between the upper and lower levels. We shall see how we can reconcile the two approaches when we consider the effects of damping in Section 9.5.2.

9.2.3 The density matrix

More advanced treatments of the phenomena described in this chapter tend to make use of the **density matrix**, $\boldsymbol{\rho}$. The elements of the density matrix are defined by:

$$\rho_{ij} = \langle c_i c_j^* \rangle, \tag{9.6}$$

where c_i is the wave function amplitude for the ith quantum level, and the subscripts i and j run over all the quantum states of the atom. The symbol $\langle \cdots \rangle$ indicates that we take the average value for the ensemble in a many-particle system.

Let us consider the density matrix of the two-level atoms that we are considering here. In general, the density matrix takes the form:

$$\boldsymbol{\rho} = \begin{pmatrix} \langle |c_1|^2 \rangle & \langle c_1 c_2^* \rangle \\ \langle c_1^* c_2 \rangle & \langle |c_2|^2 \rangle \end{pmatrix}. \tag{9.7}$$

The key difference between statistical mixtures and coherent superpositions is the presence of **off-diagonal terms** in the density matrix, namely ρ_{12} and ρ_{21}. In the case of a statistical mixture, each individual atom will either have $|c_1| = 1$ and $|c_2| = 0$ or vice versa. The off-diagonal terms are therefore zero, and the density matrix for the ensemble is of the form:

$$\boldsymbol{\rho} = \begin{pmatrix} N_1/N_0 & 0 \\ 0 & N_2/N_0 \end{pmatrix}. \tag{9.8}$$

Atoms in coherent superposition states, by contrast, have wave functions in which both $|c_1|$ and $|c_2|$ are non-zero, giving non-zero off-diagonal elements. In this case, the density matrix takes the form given in eqn 9.7 with all four elements non-zero.

We shall make no further use of the density matrix in this book. In simple systems such as two-level atoms, it suffices to discuss the behaviour

explicitly in terms of the wave function amplitudes rather than the density matrix. We mention ρ_{ij} here for the sake of completeness, and also to identify the importance of off-diagonal terms, which are central to the whole concept of superposition states.

9.3 The time-dependent Schrödinger equation

Having covered the preliminary concepts, we can now get on with the main business of the chapter. Our objective is to solve the time-dependent Schrödinger equation for a two-level atom in the presence of the light. In other words, we must solve:

$$\hat{H}\Psi = \mathrm{i}\hbar\frac{\partial\Psi}{\partial t}, \tag{9.9}$$

for an atom with two energy levels E_1 and E_2 in the presence of a light wave of angular frequency ω. We shall assume that the light is very close to resonance with the transition, so that

$$\omega = \omega_0 + \delta\omega, \tag{9.10}$$

where

$$\omega_0 = (E_2 - E_1)/\hbar, \tag{9.11}$$

and $\delta\omega \ll \omega_0$. Exact resonance thus corresponds to $\delta\omega = 0$.

We start by splitting the Hamiltonian into a time-independent part $\hat{H}_0$ which describes the atom in the dark, and a perturbation term $\hat{V}(t)$ which accounts for the light–atom interaction:

$$\hat{H} = \hat{H}_0(\boldsymbol{r}) + \hat{V}(t). \tag{9.12}$$

Since we are dealing with a two-level atom, there will be two solutions for the unperturbed system:

$$\hat{H}_0\Psi_i = \mathrm{i}\hbar\frac{\partial\Psi_i}{\partial t}, \tag{9.13}$$

with

$$\Psi_i(\boldsymbol{r},t) = \psi_i(\boldsymbol{r})\exp(-\mathrm{i}E_i t/\hbar) \quad \{i = 1,2\}, \tag{9.14}$$

and

$$\hat{H}_0(\boldsymbol{r})\psi_i(\boldsymbol{r}) = E_i\,\psi_i(\boldsymbol{r}) \quad \{i = 1,2\}. \tag{9.15}$$

The general solution to the time-dependent Schrödinger equation (eqn 9.9) is:

$$\Psi(\boldsymbol{r},t) = \sum_i c_i(t)\psi_i(\boldsymbol{r})\exp(-\mathrm{i}E_i t/\hbar), \tag{9.16}$$

where the subscript i runs over all the eigenstates of the system. In the case of a two-level atom, this reduces to:

$$\Psi(\boldsymbol{r},t) = c_1(t)\psi_1(\boldsymbol{r})\mathrm{e}^{-\mathrm{i}E_1 t/\hbar} + c_2(t)\psi_2(\boldsymbol{r})\mathrm{e}^{-\mathrm{i}E_2 t/\hbar}. \tag{9.17}$$

On substituting this wave function into eqn 9.9 with $\hat{H}$ given by eqn 9.12, we obtain:

$$(\hat{H}_0 + \hat{V})\left(c_1\psi_1 \mathrm{e}^{-\mathrm{i}E_1 t/\hbar} + c_2\psi_2 \mathrm{e}^{-\mathrm{i}E_2 t/\hbar}\right)$$
$$= \mathrm{i}\hbar\left((\dot{c}_1 - \mathrm{i}E_1 c_1/\hbar)\psi_1 \mathrm{e}^{-\mathrm{i}E_1 t/\hbar} + (\dot{c}_2 - \mathrm{i}E_2 c_2/\hbar)\psi_2 \mathrm{e}^{-\mathrm{i}E_2 t/\hbar}\right). \quad (9.18)$$

Now eqn 9.15 implies that

$$\hat{H}_0\left(c_1\psi_1 \mathrm{e}^{-\mathrm{i}E_1 t/\hbar} + c_2\psi_2 \mathrm{e}^{-\mathrm{i}E_2 t/\hbar}\right)$$
$$= \left(c_1 E_1\psi_1 \mathrm{e}^{-\mathrm{i}E_1 t/\hbar} + c_2 E_2\psi_2 \mathrm{e}^{-\mathrm{i}E_2 t/\hbar}\right), \quad (9.19)$$

so that we can cancel several of the terms in eqn 9.18 to obtain:

$$c_1\hat{V}\psi_1 \mathrm{e}^{-\mathrm{i}E_1 t/\hbar} + c_2\hat{V}\psi_2 \mathrm{e}^{-\mathrm{i}E_2 t/\hbar} = \mathrm{i}\hbar\dot{c}_1\psi_1 \mathrm{e}^{-\mathrm{i}E_1 t/\hbar} + \mathrm{i}\hbar\dot{c}_2\psi_2 \mathrm{e}^{-\mathrm{i}E_2 t/\hbar}. \quad (9.20)$$

On multiplying by ψ_1^*, integrating over space, and making use of the orthonormality of the eigenfunctions, which requires that:

$$\int \psi_i^*\psi_j \,\mathrm{d}^3\boldsymbol{r} = \delta_{ij}, \quad (9.21)$$

where δ_{ij} is the Kronecker delta function, we find that:

$$\dot{c}_1(t) = -\frac{\mathrm{i}}{\hbar}\left(c_1(t)V_{11} + c_2(t)V_{12}\,\mathrm{e}^{-\mathrm{i}\omega_0 t}\right), \quad (9.22)$$

where

$$V_{ij}(t) \equiv \langle i|\hat{V}(t)|j\rangle = \int \psi_i^*\hat{V}(t)\psi_j \,\mathrm{d}^3\boldsymbol{r}. \quad (9.23)$$

Similarly, on multiplying by ψ_2^* and integrating, we find that:

$$\dot{c}_2(t) = -\frac{\mathrm{i}}{\hbar}\left(c_1(t)V_{21}\mathrm{e}^{\mathrm{i}\omega_0 t} + c_2(t)V_{22}\right). \quad (9.24)$$

To proceed further we must consider the explicit form of the perturbation $\hat{V}$. In the semi-classical approach, the light–atom interaction is given by the energy shift of the atomic dipole in the electric field of the light:

$$\hat{V}(t) = e\boldsymbol{r}\cdot\boldsymbol{\mathcal{E}}(t). \quad (9.25)$$

See eqns 4.14 and 4.15. Note that e is the *magnitude* of the electron charge.

We arbitrarily choose the x-axis as the direction of the polarization so that we can write:

$$\boldsymbol{\mathcal{E}}(t) = (\mathcal{E}_0, 0, 0)\cos\omega t, \quad (9.26)$$

where $\mathcal{E}_0$ is the amplitude of the light wave. The perturbation then simplifies to:

$$\hat{V}(t) = ex\mathcal{E}_0\cos\omega t$$
$$= \frac{ex\mathcal{E}_0}{2}\left(\mathrm{e}^{\mathrm{i}\omega t} + \mathrm{e}^{-\mathrm{i}\omega t}\right), \quad (9.27)$$

and the perturbation matrix elements are given by:

$$V_{ij}(t) = \frac{e\mathcal{E}_0}{2}\left(\mathrm{e}^{\mathrm{i}\omega t} + \mathrm{e}^{-\mathrm{i}\omega t}\right)\int \psi_i^* x \psi_j \,\mathrm{d}^3\boldsymbol{r}. \tag{9.28}$$

Now the **dipole matrix element** μ_{ij} is given by:

$$\mu_{ij} = -e\int \psi_i^* x \psi_j \,\mathrm{d}^3\boldsymbol{r} \equiv -e\langle i|x|j\rangle, \tag{9.29}$$

so that we can write:

$$V_{ij}(t) = -\frac{\mathcal{E}_0}{2}\left(\mathrm{e}^{\mathrm{i}\omega t} + \mathrm{e}^{-\mathrm{i}\omega t}\right)\mu_{ij}. \tag{9.30}$$

Since x is an odd parity operator and atomic states have either even or odd parities (see Section 4.3), it must be the case that $\mu_{11} = \mu_{22} = 0$. Moreover, the dipole matrix element represents a measurable quantity and must be real, which implies that $\mu_{21} = \mu_{12}$, because $\mu_{21} = \mu_{12}^*$. With these simplifications, eqns 9.22 and 9.24 reduce to:

$$\begin{aligned}\dot{c}_1(t) &= \mathrm{i}\frac{\mathcal{E}_0\mu_{12}}{2\hbar}\left(\mathrm{e}^{\mathrm{i}(\omega-\omega_0)t} + \mathrm{e}^{-\mathrm{i}(\omega+\omega_0)t}\right)c_2(t),\\ \dot{c}_2(t) &= \mathrm{i}\frac{\mathcal{E}_0\mu_{12}}{2\hbar}\left(\mathrm{e}^{-\mathrm{i}(\omega-\omega_0)t} + \mathrm{e}^{\mathrm{i}(\omega+\omega_0)t}\right)c_1(t).\end{aligned} \tag{9.31}$$

The Rabi frequency defined here is an *angular* frequency.

We now introduce the **Rabi frequency** defined by:

$$\Omega_\mathrm{R} = |\mu_{12}\mathcal{E}_0/\hbar|. \tag{9.32}$$

The phase factors that might result from using the modulus sign to ensure that the Rabi frequency defined in eqn 9.32 is real and positive have no physical significance and have been suppressed in eqn 9.33.

We then finally obtain:

$$\begin{aligned}\dot{c}_1(t) &= \frac{\mathrm{i}}{2}\Omega_\mathrm{R}\left(\mathrm{e}^{\mathrm{i}(\omega-\omega_0)t} + \mathrm{e}^{-\mathrm{i}(\omega+\omega_0)t}\right)c_2(t),\\ \dot{c}_2(t) &= \frac{\mathrm{i}}{2}\Omega_\mathrm{R}\left(\mathrm{e}^{-\mathrm{i}(\omega-\omega_0)t} + \mathrm{e}^{\mathrm{i}(\omega+\omega_0)t}\right)c_1(t)\,.\end{aligned} \tag{9.33}$$

These are the equations that we must solve to understand the behaviour of the atom in the light field. It turns out that there are two distinct types of solution that can be found, which correspond to the **weak-field limit** and the **strong-field limit** respectively. We consider the weak-field limit first.

9.4 The weak-field limit: Einstein's *B* coefficient

The weak-field limit applies to low-intensity light sources such as black-body lamps. We assume that the atom is initially in the lower level and that the lamp is turned on at $t = 0$. This implies that $c_1(0) = 1$ and $c_2(0) = 0$.

With a low-intensity source, the electric field amplitude will be small and the perturbation weak. The number of transitions expected is

therefore small, and it will always be the case that $c_1(t) \gg c_2(t)$. In these conditions we can put $c_1(t) = 1$ for all t, so that eqn 9.33 reduces to:

$$\dot{c}_1(t) = 0,$$
$$\dot{c}_2(t) = \frac{\mathrm{i}}{2}\Omega_\mathrm{R}\left(\mathrm{e}^{-\mathrm{i}(\omega-\omega_0)t} + \mathrm{e}^{\mathrm{i}(\omega+\omega_0)t}\right). \tag{9.34}$$

The solution for $c_2(t)$ with $c_2(0) = 0$ is:

$$c_2(t) = \frac{\mathrm{i}}{2}\Omega_\mathrm{R}\left[\frac{\mathrm{e}^{-\mathrm{i}\delta\omega t} - 1}{-\mathrm{i}\delta\omega} + \frac{\mathrm{e}^{\mathrm{i}(\omega+\omega_0)t} - 1}{\mathrm{i}(\omega+\omega_0)}\right], \tag{9.35}$$

where we made use of eqn 9.10. According to the **rotating wave approximation**, we now neglect the second term in eqn 9.35. This is justified by the fact that since $\delta\omega \ll (\omega + \omega_0)$, the second term is much smaller than the first. After some manipulation we find:

$$|c_2(t)|^2 = \left(\frac{\Omega_\mathrm{R}}{2}\right)^2 \left(\frac{\sin \delta\omega t/2}{\delta\omega/2}\right)^2. \tag{9.36}$$

When the beam is tuned to exact resonance with the transition, $\delta\omega$ is equal to zero. We thus find:

$$|c_2(t)|^2 = \left(\frac{\Omega_\mathrm{R}}{2}\right)^2 t^2, \tag{9.37}$$

leading to the unsatisfactory conclusion that the probability that the atom is in the upper level increases as t^2. This is at odds with the Einstein approach in which the transition probability is time-independent, so that $|c_2(t)|^2$ should increase linearly with time.

The way around this apparent contradiction is to re-examine the assumptions of our analysis. We have assumed throughout that the atomic transition line is perfectly sharp. However, we know in fact that all spectral lines have a finite width $\Delta\omega$. (See Section 4.4.) Furthermore, we are considering the interaction between the atom and a broad-band source such as a black-body lamp. Such a broad-band source can be specified by the spectral energy density $u(\omega)$, which must satisfy:

$$\frac{1}{2}\epsilon_0 \mathcal{E}_0^2 = \int u(\omega)\,\mathrm{d}\omega. \tag{9.38}$$

We therefore integrate eqn 9.36 over the spectral line:

$$|c_2(t)|^2 = \frac{\mu_{12}^2}{2\epsilon_0\hbar^2}\int_{\omega_0-\Delta\omega/2}^{\omega_0+\Delta\omega/2} u(\omega)\left(\frac{\sin(\omega-\omega_0)t/2}{(\omega-\omega_0)/2}\right)^2 \mathrm{d}\omega, \tag{9.39}$$

where we used eqns 9.32 and 9.38 to substitute for Ω_R and $\mathcal{E}_0^2$, respectively. We now make the approximation that the spectral line is sharp compared to the broad-band spectrum of the lamp, so that $u(\omega)$ does not vary significantly within the integral. This allows us to replace $u(\omega)$ by a constant value $u(\omega_0)$, and thus to evaluate the integral. The limiting value for $t\Delta\omega \to \infty$ is $u(\omega_0)2\pi t$. Hence we finally obtain:

$$|c_2(t)|^2 = \frac{\pi}{\epsilon_0\hbar^2}\,\mu_{12}^2\,u(\omega_0)\,t, \tag{9.40}$$

which is a much more satisfactory result because it implies that the probability that the atom is in the upper level increases linearly with time.

We can now relate eqn 9.40 to the Einstein B coefficient defined by:

$$\frac{\mathrm{d}N_2}{\mathrm{d}t} = B_{12}^{\omega} u(\omega_0) N_1 \,, \tag{9.41}$$

Note that the energy density can be defined either in terms of the frequency ν or the angular frequency ω, with the two values differing by a factor 2π. Two different Einstein B coefficients B_{12}^{ν} and B_{12}^{ω} can be defined accordingly, with $B_{12}^{\nu} = B_{12}^{\omega}/2\pi$. See eqn 9.43.

which implies that the transition probability per unit time per atom is $B_{12}^{\omega} u(\omega_0)$. In the analysis leading up to eqn 9.33, we assumed that the atomic dipole moment was aligned parallel to the polarization vector of the light. However, in a gas of atoms, the direction of the atomic dipoles will be random. If the angle between the polarization and a particular dipole is θ, then we need to take the average of $(\mu_{12}\cos\theta)^2$ for all the atoms in the gas. On using $\langle\cos^2\theta\rangle = 1/3$, we then replace μ_{12}^2 by $\mu_{12}^2/3$ throughout to obtain the transition probability rate W_{12}:

$$W_{12} \equiv B_{12}^{\omega} u(\omega_0) = \frac{|c_2|^2}{t} = \frac{\pi}{3\epsilon_0 \hbar^2} \mu_{12}^2 u(\omega_0), \tag{9.42}$$

which finally gives:

$$\begin{aligned} B_{12}^{\omega} &= \frac{\pi}{3\epsilon_0 \hbar^2} \mu_{12}^2, \\ B_{12}^{\nu} &= \frac{1}{6\epsilon_0 \hbar^2} \mu_{12}^2. \end{aligned} \tag{9.43}$$

This shows that the weak-field limit is equivalent to the Einstein analysis, and allows us to calculate explicit values of the B coefficient from the atomic wave functions.

Example 9.1 Calculate the Einstein B coefficient B_{12}^{ω} for the 1s $\rightarrow$ 2p atomic transition in hydrogen for light polarized along the z-axis.

Solution

For light polarized along the z-axis the selection rules permit $\Delta m = 0$ transitions only. (See Section 4.3.) Hence we are considering the transition between two hydrogenic states with quantum numbers (n, l, m_l) of (1,0,0) and (2,1,0), respectively. The initial and final wave functions are therefore:

$$\begin{aligned} \psi_1(r,\theta,\phi) &= \frac{1}{\sqrt{\pi}} \left(\frac{1}{a_0}\right)^{3/2} \mathrm{e}^{-r/a_0}, \\ \psi_2(r,\theta,\phi) &= \frac{1}{\sqrt{\pi}} \left(\frac{1}{2a_0}\right)^{5/2} r\cos\theta\, \mathrm{e}^{-r/2a_0}, \end{aligned}$$

where a_0 is the Bohr radius. In analogy to eqn 9.29, the transition dipole moment μ_{12} for z-polarized light is given by:

$$\begin{aligned}\mu_{12} &= -e\int \psi_1^* z\psi_2 \,\mathrm{d}^3\boldsymbol{r} \\ &= -e\int_{r=0}^{\infty}\int_{\theta=0}^{\pi}\int_{\phi=0}^{2\pi} \psi_1^*\, r\cos\theta\,\psi_2\, r^2\sin\theta\,\mathrm{d}r\,\mathrm{d}\theta\,\mathrm{d}\phi \\ &= -\frac{128\sqrt{2}}{243}ea_0 \\ &= -6.32\times10^{-30}\,\mathrm{C\,m}.\end{aligned}$$

We then obtain $B_{12}^{\omega} = 4.25\times10^{20}\,\mathrm{m^3\,rad\,J^{-1}\,s^{-2}}$ on substituting into eqn 9.43.

9.5 The strong-field limit: Rabi oscillations

9.5.1 Basic concepts

In the previous section we assumed that the light field was weak so that the population of the excited state was always small and the approximation $c_1(t) \approx 1$ was valid for all t. This allowed us to find a simple solution to eqn 9.33. We now wish to return to the more general case in which the population of the upper level is significant. It is intuitively obvious that this condition applies when the light–atom interaction is strong. In other words, we are dealing with the case of strong electric fields, such as those found in powerful laser beams.

In order to find a solution to eqn 9.33 in the strong-field limit we make two simplifications. First, we apply the rotating wave approximation to neglect the terms that oscillate at $\pm(\omega+\omega_0)$, as in the previous section. Second, we only consider the case of exact resonance with $\delta\omega = 0$. With these simplifications, eqn 9.33 reduces to:

The mathematics of non-exact resonance is more complicated, and is considered in Exercise 9.5.

$$\begin{aligned}\dot{c}_1(t) &= \frac{\mathrm{i}}{2}\Omega_{\mathrm{R}}c_2(t), \\ \dot{c}_2(t) &= \frac{\mathrm{i}}{2}\Omega_{\mathrm{R}}c_1(t).\end{aligned} \tag{9.44}$$

We differentiate the first line and substitute from the second to find:

$$\ddot{c}_1 = \frac{\mathrm{i}}{2}\Omega_{\mathrm{R}}\dot{c}_2 = \left(\frac{\mathrm{i}}{2}\Omega_{\mathrm{R}}\right)^2 c_1. \tag{9.45}$$

We thus obtain

$$\ddot{c}_1 + \left(\frac{\Omega_{\mathrm{R}}}{2}\right)^2 c_1 = 0, \tag{9.46}$$

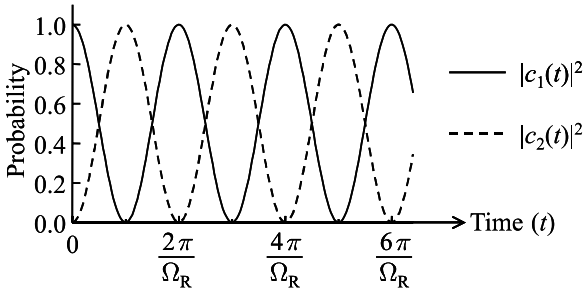

Fig. 9.4 Probability for finding the atom in either the upper or lower level in the strong-field limit in the absence of damping. The electron oscillates back and forth between the two levels at the Rabi angular frequency, Ω_R. This phenomenon is either called Rabi flopping or Rabi oscillation.

which describes oscillatory motion at angular frequency $\Omega_R/2$. If the particle is in the lower level at $t = 0$ so that $c_1(0) = 1$ and $c_2(0) = 0$, the solution is:

$$c_1(t) = \cos(\Omega_R t/2),$$
$$c_2(t) = \mathrm{i}\sin(\Omega_R t/2). \tag{9.47}$$

The probabilities for finding the electron in the upper or lower levels are then given by:

$$|c_1(t)|^2 = \cos^2(\Omega_R t/2),$$
$$|c_2(t)|^2 = \sin^2(\Omega_R t/2). \tag{9.48}$$

The time dependence of these probabilities is shown in Fig. 9.4. At $t = \pi/\Omega_R$ the electron is in the upper level, whereas at $t = 2\pi/\Omega_R$ it is back in the lower level. The process then repeats itself with a period equal to $2\pi/\Omega_R$. The electron thus oscillates back and forth between the lower and upper levels at a frequency equal to $\Omega_R/2\pi$. This oscillatory behaviour in response to the strong-field is called **Rabi oscillation** or **Rabi flopping**.

See I. I. Rabi, *Phys. Rev.* **51**, 652 (1937). Rabi's original derivation applied to oscillating electromagnetic fields tuned to resonance with the Zeeman-split levels of a spin-1/2 nucleus. The RF field tips the spin vector from down to up and then back to down again, a process entirely equivalent to the Rabi flopping considered here. Rabi's work was the precursor to modern NMR techniques, and its importance was recognized by the awarding of the Nobel Prize for Physics in 1944. A brief discussion of the phenomenon of NMR may be found in Appendix E.

When the light is not exactly resonant with the transition, it can be shown that the second line of eqn 9.48 is modified to (see Exercise 9.5):

$$|c_2(t)|^2 = \frac{\Omega_R^2}{\Omega^2}\sin^2(\Omega t/2), \tag{9.49}$$

where

$$\Omega^2 = \Omega_R^2 + \delta\omega^2, \tag{9.50}$$

$\delta\omega$ being the detuning. This shows that the frequency of the Rabi oscillations increases but their amplitude decreases as the light is tuned away from resonance.

For transitions in the visible-frequency range, the experimental observation of Rabi flopping requires powerful laser beams. In many cases, these lasers will be pulsed, so that the electric field amplitude $\mathcal{E}_0$ varies with time. Equation 9.32 then tells us that the Rabi frequency $\Omega_R/2\pi$

also varies with time, and so it is useful to define the **pulse area** Θ according to:

$$\Theta = \left| \frac{\mu_{12}}{\hbar} \int_{-\infty}^{+\infty} \mathcal{E}_0(t)\, \mathrm{d}t \right|. \tag{9.51}$$

The pulse area is a dimensionless parameter which is determined by the pulse energy and serves the same purpose as $\Omega_R t$ in the analysis above. A pulse which has an area equal to π is called a **π-pulse**. An atom in the ground state with $c_1 = 1$ at $t = 0$ will thus be promoted to the excited state with $c_2 = 1$ by a π-pulse, but will end up back in the ground state if it interacts with a 2π-pulse. We shall see in Section 9.6 that the pulse area can be given a geometric interpretation in terms of rotation angles of the Bloch vector.

The startling oscillatory behaviour predicted by eqn 9.48 has been observed in many systems, as will be discussed in Section 9.5.3. The following example illustrates the time-scales involved in Rabi flopping processes, and introduces the importance of damping effects, which are considered next.

Example 9.2 A powerful beam of light is incident on a gas of monatomic hydrogen and is tuned to resonance with the 1s $\rightarrow$ 2p transition at 137 nm.

(a) Calculate the Rabi oscillation period when the optical intensity is 10 kW m^{-2} and the light is polarized in the z-direction.

(b) Calculate the optical intensity required to make the Rabi oscillation period equal to the radiative lifetime of the 2p level, namely 1.6 ns.

Solution

(a) The atomic dipole moment for this transition was calculated in Example 9.1 to be $-0.74ea_0 = -6.32 \times 10^{-30}$ C m. The intensity of a light beam is related to its electric field amplitude according to (see eqn 2.28):

$$I = \frac{1}{2} c\epsilon_0 n \mathcal{E}_0^2, \tag{9.52}$$

where n is the refractive index of the medium. In a gas we may take $n \approx 1$, and so we find $\mathcal{E}_0 = 2.7 \times 10^3$ V m^{-1}. On substituting into eqn 9.32, we find the Rabi frequency:

$$\begin{aligned} \Omega_R &= |-6.32 \times 10^{-30} \times 2.7 \times 10^3/\hbar| \\ &= 1.6 \times 10^8 \text{ rad s}^{-1}. \end{aligned}$$

Hence the Rabi flopping period is equal to $2\pi/\Omega_R = 38$ ns.

(b) A Rabi oscillation period of 1.6 ns corresponds to $\Omega_R = 3.9 \times 10^9$ rad s^{-1}. From eqn 9.32 we calculate $\mathcal{E}_0 = 6.5 \times 10^4$ V m^{-1}, and hence from eqn 9.52 we find $I = 5.7$ MW m^{-2}.

9.5.2 Damping

Example 9.2 illustrates why it is difficult to observe Rabi oscillations in the laboratory. At low powers, the oscillation period is longer than the radiative lifetime, and we would expect random spontaneous emission events to destroy the coherence of the superposition states, and hence curtail the oscillations. We thus have to work at higher powers to shorten the Rabi flopping period, which can be difficult to achieve in practice.

Spontaneous emission is just one example of a **damping** mechanism for the Rabi oscillations. We shall now see that the consideration of damping is very important for determining the experimental conditions under which Rabi oscillations can be observed. Damping also provides a way to reconcile the rather counter-intuitive phenomenon of Rabi oscillations with the more familiar concept of transition rates which form the basis of the Einstein model.

The damping processes for coherent phenomena such as Rabi flopping are traditionally characterized by two time constants, T_1 and T_2, following Bloch's treatment of nuclear magnetic resonance. (See Appendix E, Section E.3.) As will be explained in Section 9.6, these two types of damping are sometimes called **longitudinal relaxation** and **transverse relaxation**, respectively. In physical terms, T_1 damping is essentially determined by **population decay**, whereas T_2 damping is related to **dephasing** processes.

The T_1 (longitudinal) damping processes are the simplest to understand. If the atom is in the excited state, it will have a spontaneous tendency to decay to lower levels. The decay processes occur stochastically (i.e. according to probabilistic laws) and randomly break the coherence of the electronic wave function. Hence a spontaneous decay would permanently interrupt the Rabi flopping, which relies on the coherence of the superposition states. The rate of these types of damping process is governed by the lifetime τ of the upper level, which itself is determined by both the radiative and non-radiative decay rates:

$$\frac{1}{\tau} = \frac{1}{\tau_{\mathrm{R}}} + \frac{1}{\tau_{\mathrm{NR}}}. \tag{9.53}$$

The upper limit on T_1 is thus set by the radiative lifetime τ_{R} of the excited state, which includes transitions both to the resonant lower level and to other non-resonant levels that have been neglected so far in the two-level atom approximation.

The T_2 (transverse) damping processes are more subtle to understand. It will frequently be the case that an atom in the excited state undergoes an elastic (i.e. energy conserving) or near-elastic collision which breaks the phase of the wave function without altering the population of the excited state. These scattering processes can occur by a number of different mechanisms. In a gas, collisions can occur between the atoms or with the walls of the vessel, whereas in a solid there can be interactions with impurities or lattice vibrations (phonons). By randomizing

the phase of the wave function, the collisions destroy any effects such as Rabi flopping which rely on phase coherence.

It is thus apparent that dephasing can occur by two distinct mechanisms: population decay and population-conserving scattering processes. We can therefore write the total dephasing rate, in the presence of both types of decoherence mechanisms, as:

$$\frac{1}{T_2} = \frac{1}{2T_1} + \frac{1}{T_2'}. \tag{9.54}$$

See Allen and Eberly (1975, eqn 3.29), with $\Delta = 0$ and $b \equiv 1/T_2$. The value of T_2' in eqn 9.54 differs from Allen and Eberly's by a factor of two. This change of notation has been made so that, in the limit, $T_2' \ll T_1$, we obtain $T_2 = T_2'$ rather than $T_2 = 2T_2'$.

The first term on the right-hand side accounts for dephasing by population decay, while the second accounts for dephasing by population-conserving scattering. The latter process is sometimes called 'pure dephasing' to distinguish it from the dephasing caused by population decay.

It will often be the case, especially in solids at room temperature, that the pure dephasing rate is much faster than the population decay rate (i.e. $T_2' \ll T_1$), and so the decoherence is governed primarily by scattering processes. On the other hand, it can sometimes be the case that $T_2' \gg T_1$, so that the decoherence is then governed primarily by T_1, which itself is determined by the lifetime of the upper level.

Pure dephasing processes can usually be suppressed, to a greater or lesser extent, by cooling the system to very low temperatures. Such techniques are important for applications that require long coherence times, for example, quantum computation: see Section 13.4.

Having considered the processes that cause dephasing in quantum systems, we can now study the detailed effects of damping on Rabi oscillations. It can be shown that if the damping rate is γ, the probability that the electron is in the upper level, namely $|c_2(t)|^2$, is given by:

See, for example, Loudon (2000, § 2.8).

$$|c_2(t)|^2 = \frac{1}{2(1+2\xi^2)}\left[1 - \left(\cos\Omega' t + \frac{3\xi}{(4-\xi^2)^{1/2}}\sin\Omega' t\right)\exp\left(-\frac{3\gamma t}{2}\right)\right], \tag{9.55}$$

where

$$\xi = \gamma/\Omega_R,$$
$$\Omega' = \Omega_R\sqrt{1-\xi^2/4}. \tag{9.56}$$

It is easily verified that this formula reduces to the undamped case given in eqn 9.48 when $\gamma = 0$.

Figure 9.5 shows graphs of $|c_2(t)|^2$ from eqn 9.55 for three different values of the damping constant. The dotted line shows the undamped case with $\gamma = 0$ considered previously in Section 9.5.1. The two other graphs correspond to light damping ($\gamma/\Omega_\mathrm{R} = 0.1$) and strong damping ($\gamma/\Omega_\mathrm{R} = 1$), respectively. Let us consider the case of light damping first. The electron performs a few damped oscillations and then approaches the asymptotic limit with $|c_1|^2 = |c_2|^2 = 1/2$. This asymptotic limit is exactly the behaviour we would have expected from the Einstein analysis of a pure two-level system in the strong-field limit. At high optical power levels the spontaneous emission rate is negligible and the rates of stimulated emission and absorption eventually equal out, leading to identical upper and lower level populations. (See Exercise 9.6.)

Now consider the behaviour for strong damping. This is effectively equivalent to the weak-field limit, because we can always make γ/Ω_R

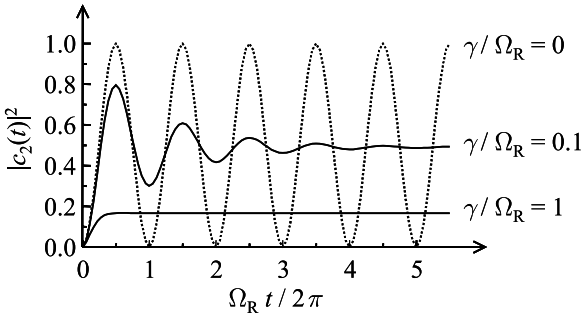

Fig. 9.5 Damped Rabi oscillations for two values of the ratio of the damping rate γ to the Rabi oscillation frequency Ω_R. The dotted curve shows the oscillations when no damping is present.

large by turning down the electric field of the light beam. (See eqn 9.32.) No oscillations are observed, and the asymptotic value of $|c_2|^2$ for very large damping rates (i.e. $\xi \gg 1$) is given by:

$$|c_2|^2 \to \xi^{-2}/4 = \Omega_R^2/4\gamma^2 = \frac{\mu_{12}^2 \mathcal{E}_0^2}{4\hbar^2\gamma^2}. \tag{9.57}$$

This is consistent with our previous analysis of the weak-field limit, where we found that the transition probability is proportional to the square of both the dipole moment and the electric field (see eqn 9.40, and recall that $u(\omega_0) \propto \mathcal{E}_0^2$.) The time independence of eqn 9.57 compared to eqn 9.40 can be explained by the fact that the former is an asymptotic limit with damping included. In fact, if we solve for the asymptotic populations in the Einstein analysis, we find that N_2 is also independent of time, with $N_2/N_0 \to B_{12}^{\omega} u_\omega g_\omega(\omega_0)/A_{21}$, where u_ω is the energy density of the radiation and $g_\omega(\omega)$ is the spectral lineshape function. (See Exercise 9.6.) The appearance of A_{21} in the denominator of the asymptotic limit explains one of the factors of γ in the denominator of eqn 9.57, since the damping rate would just be proportional to $\tau_R^{-1} \equiv A_{21}$ for an isolated two-level system. The other factor of γ comes from the fact that the radiative lifetime also causes line broadening.

This simple discussion shows how the inclusion of damping allows us to understand the evolution of the behaviour as the electric field strength is increased. At low fields, we are in the strongly damped regime where there are discrete transitions and the Einstein analysis is valid. As the field is increased, the ratio of the damping rate to the Rabi frequency decreases, and we can eventually reach the case where the oscillations are observable.

9.5.3 Experimental observations of Rabi oscillations

It is apparent from Fig. 9.5 that Rabi oscillations are strongly damped except when

$$\Omega_R \equiv |\mu_{12}\mathcal{E}_0/\hbar| \gg \gamma\,. \tag{9.58}$$

In gases, the damping rate depends on the collision rate and the radiative lifetime, which gives typical values of γ for optical-frequency transitions in the range 10^7–10^9 s^{-1}. In solids the dephasing times are often shorter due to phonon scattering and scattering by free charge carriers, and γ

can be as high as 10^{12} s^{-1}. These high damping rates make the task of demonstrating Rabi oscillations somewhat difficult, which explains why they are not routinely observed. The observation of the oscillations in the time domain requires a time resolution shorter than $1/\Omega_R$, while the short Rabi oscillation periods demanded by eqn 9.58 require large electric field amplitudes. These conditions are usually satisfied by using high-power pulsed lasers with pulse durations shorter than γ^{-1}.

The first experimental evidence of Rabi oscillations was of an indirect nature and came from the observation of **self-induced transparency** by McCall and Hahn in 1969. They realized that if the pulse area defined in eqn 9.51 is equal to 2π, then the atoms are left in the ground state at the end of the pulse. This implies that there is no net absorption, and so a medium that absorbs strongly at low powers would become transparent to a 2π-pulse: hence the name 'self-induced transparency'. The condition to observe the phenomenon is that the pulse duration should be shorter than the damping time, and that the pulse area should be equal to an integer multiple of 2π. McCall and Hahn performed their experiments on the absorption of a ruby crystal excited resonantly with nanosecond pulses from a ruby laser. The ruby crystal was held at 4.2 K in a liquid helium cryostat to suppress damping by phonon scattering. They confirmed that the crystal did indeed become more transparent as the pulse area (determined by the energy of the pulse) approached 2π, although some deviations from the simple theory were observed due to the non-plane-wave nature of the laser beam.

See S. L. McCall and E. L. Hahn, *Phys. Rev.* **183**, 457 (1969).

The first direct evidence of Rabi oscillations came from experiments performed in the 1970s. In 1972–3 Gibbs reported on the fluorescence emitted by Rb atoms excited resonantly by short pulses from a mercury laser. By placing the Rb atoms in a superconducting magnet, one of the hyperfine components of the $M_J = -1/2 \rightarrow +1/2$ line of the $5\ ^2S_{1/2} \rightarrow 5\ ^2P_{1/2}$ transition with a dipole moment of 1.45×10^{-29} C m could be tuned to resonance with the laser by the Zeeman effect, as shown in Fig. 9.6(a). The upper level could decay either to the $+1/2$ or $-1/2$ levels of the 5s state, with radiative lifetimes of 42 and 84 ns, respectively. This gave a total radiative lifetime of $(1/42 + 1/84)^{-1} = 28$ ns. With a low density of atoms to prevent dephasing by collisions, the right conditions to observe Rabi flopping were present for pulses significantly shorter than 28 ns. The oscillations were then detected by measuring the fluorescence from the upper level as a function of the pulse area Θ.

See H. M. Gibbs, *Phys. Rev. Lett.* **29**, 459 (1972) and *Phys. Rev. A* **8**, 446 (1973).

The fine structure doublet for transitions from the first excited state to the ground state of an alkali atom are often called the D lines. The D_1 and D_2 lines originate from the $^2P_{1/2}$ and $^2P_{3/2}$ levels respectively. See Fig. 3.3.

The results of the experiment are shown in Fig. 9.6(b). The laser operated at 794.466 nm and produced pulses of 7 ns duration. The actual signal recorded was the integrated fluorescence count rate for the time window from 22 to 72 ns after the pulse arrived. This was done to ensure that only incoherent spontaneous emission events occurring after the completion of the pulse were recorded, and was achieved by electronic gating of the photomultiplier used to detect the fluorescence. The fluorescence signal showed a clear oscillatory behaviour as a function of the pulse area. When the pulse area was equal to odd integer multiples of π (i.e. $\Theta = \pi, 3\pi, \ldots$), the atoms ended up in the excited state at the

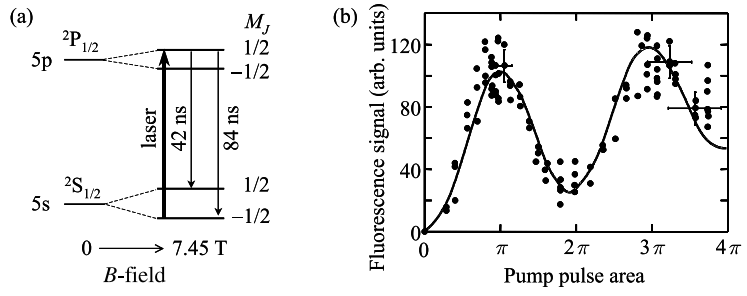

Fig. 9.6 (a) Simplified energy level scheme for the 5s → 5p D_1 transition in Rb at zero field and at $B = 7.45$ T. The wavelength of the transition at $B = 0$ is 794.764 nm, and a field of 7.45 T generated by a superconducting magnet tuned the ($M_J = -1/2 \rightarrow +1/2$) transition to resonance with a mercury laser at 794.466 nm by the Zeeman effect. The upper level can decay spontaneously by the two transitions indicated. (b) Experimental data for the fluorescence intensity from the upper level as a function of pump pulse area, using pulses with a FWHM of 7 ns. The fluorescence signal was integrated from 22 to 72 ns after the pulse arrived at $t = 0$. The solid line is a theoretical fit to the data which includes losses to other levels and also the effects of a weak tail in the laser pulses which persisted to ∼30 ns. (After H. M. Gibbs, *Phys. Rev. Lett.* **29**, 459 (1972) and *Phys. Rev. A* **8**, 446 (1973), © American Physical Society, reproduced with permission.)

completion of the pulse, and then decayed to the ground state by spontaneous emission, thus producing a strong fluorescence signal. On the other hand, when the pulse area was equal to even integer multiples of π (i.e. $\Theta = 2\pi, 4\pi, \ldots$), the atoms were in the ground state at the completion of the pulse, and no fluorescence occurred. These trends were well reproduced in the data. The fluorescence signal did not fall to exactly zero at $\Theta = 2\pi$ and 4π because of loss to the lower $M_J = +1/2$ level during the pump pulse and also due to coherent emission caused by a weak tail in the pump pulses which persisted to ∼30 ns. The solid line in Fig. 9.6(b) shows the results of a theoretical model with the loss mechanism and pulse tail effects included. It is apparent that the fit to the data is excellent, thus confirming the presence of the Rabi oscillations in the Rb atoms.

See B. R. Mollow, *Phys. Rev.* **188**, 1969 (1969).

Another important confirmation of the Rabi flopping process was the observation of **Mollow triplets**. This phenomenon, which was first considered theoretically by B. F. Mollow in 1969, is the frequency-space equivalent of the Rabi oscillations in the time domain. Mollow demonstrated that the coherent oscillatory motion of the electrons in the strong-field limit would beat with the fundamental transition angular frequency ω_0 and produce side bands in the emission spectrum at $\omega_0 \pm \Omega_R$. Hence the fluorescence spectrum would split into a triplet with components at angular frequencies of $(\omega_0 - \Omega_R)$, ω_0, and $(\omega_0 + \Omega_R)$. Several research groups confirmed this behaviour in the 1970s. The lower part of Fig. 9.7(a) shows the fluorescence spectrum measured for one of the hyperfine components of the sodium D_2 ($3\ ^2S_{1/2} \rightarrow 3\ ^2P_{3/2}$) line when the atoms are excited resonantly by intense laser light at the transition frequency. The laser light was provided by a continuous wave

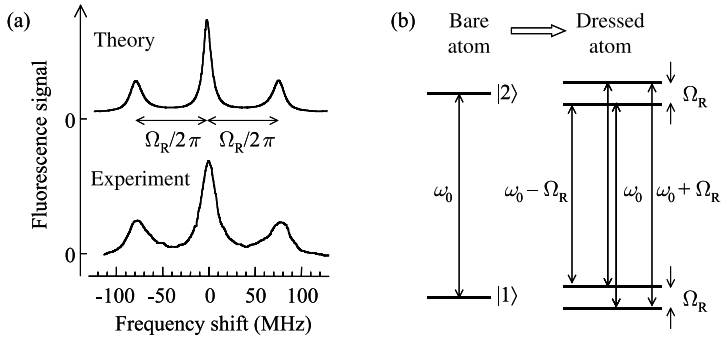

Fig. 9.7 (a) Fluorescence spectrum for one of the hyperfine components of the sodium D_2 line when excited resonantly with intense light from a dye laser. The optical intensity was 6400 Wm^{-2}, and the wavelength was 589.0 nm. The lower part of the figure shows the experimental spectrum, while the upper part shows the theoretical spectrum calculated for a Rabi frequency $\Omega_R = 2\pi \times 78$ MHz. (After R. E. Grove, F. Y. Wu, and S. Ezekiel, *Phys. Rev. A* **15**, 227 (1977), © American Physical Society, reproduced with permission.) (b) Explanation of the Mollow triplet spectrum shown in part (a) using the dressed atom picture. The AC Stark interaction between a two-level atom and an intense resonant light field splits the bare atom states into doublets separated by the Rabi frequency Ω_R. This leads to three emission lines at angular frequencies of ω_0 and $\omega_0 \pm \Omega_R$.

dye laser operating at 589.0 nm and the intensity was 6400 $\mathrm{W\,m}^{-2}$. Two peaks on either side of the central peak are clearly observed. The top part of the figure shows the theoretical spectrum calculated for a value of $\Omega_R/2\pi = 78$ MHz. The excellent agreement between theory and experiment is apparent.

Figure 9.7(b) indicates a way to interpret the Rabi oscillation phenomenon in terms of **dressed atoms**. In this picture we consider the states of the coupled resonant light–atom system rather than those of the unperturbed atom. The states of the 'bare' atom are 'dressed' by the intense resonant optical field through the **AC Stark effect** (also called the **dynamic Stark effect**). The Stark effect describes the shift of the levels of an atom in a DC electric field, and the AC Stark effect is the equivalent process for the AC electric field of a light wave. It can be shown that the AC Stark effect splits the bare atom states into doublets separated by the Rabi frequency Ω_R, as shown in Fig. 9.7(b). Hence the emission spectrum of the dressed atom consists of three lines equivalent to the Mollow triplet spectrum shown in Fig. 9.7(a).

There have been many further demonstrations of Rabi-flopping phenomena in the years following these initial experiments. Some of the most interesting recent observations have involved semiconductor quantum dot structures. (See Section D.3 in Appendix D.) Figure 9.8 shows the results for InAs quantum dots embedded within a GaAs photodiode. Figure 9.8(a) shows a schematic diagram of the device used in this experiment. Masks patterned onto the surface allowed individual quantum dots to be excited by short pulses from a mode-locked Ti:sapphire laser. The Rabi oscillations were induced by tuning the laser to the lowest energy

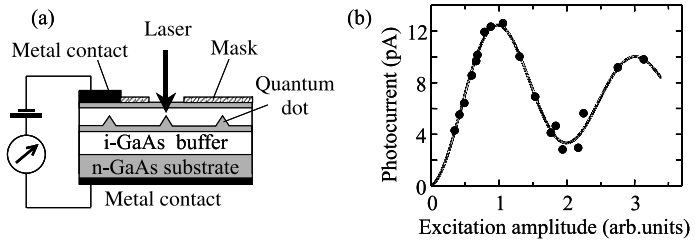

Fig. 9.8 (a) Schematic diagram of the quantum dot photodiode used to demonstrate Rabi oscillations. The device consisted of InAs quantum dots embedded within a GaAs n-i-Schottky diode structure. The device was biassed by an external DC power supply which applied a strong DC electric field to the quantum dots. Free electrons and holes excited in the quantum dots by absorption of laser light tunnel into the GaAs regions under the influence of the DC field and are then swept to the contacts to generate a photocurrent in the external circuit. A mask on the top of the device allowed individual quantum dots to be addressed by the laser beam. (b) Photocurrent measured when exciting the lowest energy transition of the quantum dots resonantly with 1 ps pulses from a Ti:sapphire laser at 1.31 eV. The excitation amplitude has been scaled so that an amplitude of unity corresponds to a π-pulse. (After A. Zrenner *et al.*, *Nature* **418**, 612 (2002), © Nature Publishing Group, reproduced with permission.)

transition of the quantum dot at 1.31 eV. This transition corresponds to the excitation of an electron from the valence band to the conduction band, and has a dipole moment of $\sim 8 \times 10^{-29}$ C m. The experiment consisted in measuring the photocurrent generated in the external circuit as a function of the laser pulse area Θ.

The results of the experiment are shown in Fig. 9.8(b). The photocurrent shows a clear oscillatory behaviour with the pulse excitation amplitude, which has been scaled so that an amplitude of unity corresponds to a pulse area of π. There are peaks for pulse areas of π and 3π, and a minimum for $\Theta = 2\pi$. The results may be understood by considering the state of the system at the completion of the pulse, in an analogous way to the discussion of the data in Fig. 9.6(b). At the end of a π or 3π pulse, the quantum dots are left with one electron in the conduction band and hence one 'hole' in the valence band. These charge carriers can then tunnel out of the quantum dot under the influence of the DC electric field of the photodiode and produce a photocurrent in the external circuit. On the other hand, after a 2π pulse the electron is back in the valence band and there are no free electrons and holes to generate a current. This is exactly what is observed.

The Rabi oscillations shown in Fig. 9.8(b) are partly damped by rapid dephasing processes. The main source of dephasing was the loss of electrons and holes due to tunnelling out of the quantum dots. This process is unavoidable, since it is an integral part of the mechanism to generate the photocurrent used to detect the Rabi oscillations. The estimated tunnelling time was $\approx$10 ps, and it was for this reason that very short pulses with a duration of only 1 ps had to be used in the experiment.

These very short time-scales highlight the difficulty in observing coherent phenomena like Rabi oscillations in the solid state.

9.6 The Bloch sphere

An arbitrary superposition state of a two-level system will have a wave function of the form given by eqn 9.2, namely:

$$|\psi\rangle = c_1|1\rangle + c_2|2\rangle. \tag{9.59}$$

The normalization condition on the wave function requires that:

$$|c_1|^2 + |c_2|^2 = 1, \tag{9.60}$$

which suggests that we can represent the state by a vector of unit length starting at the origin. This geometric interpretation of coherent superposition states is called the **Bloch representation**. The vector that describes the state is called the **Bloch vector**, and the sphere it defines is the **Bloch sphere**.

The Bloch representation was originally developed by Felix Bloch in 1946 to model NMR phenomena, and was first adapted to two-level atoms by Feynman *et al.* in 1957. The equivalence between two-level atoms and Zeeman-split nuclear spin states was noted previously in Section 9.2.1 (see Fig. 9.3) and allows us to share analytic tools such as the Bloch representation between the two subjects. Readers who are unfamiliar with NMR phenomena may therefore find it helpful to refer to Appendix E which gives a summary of the main effects.

See R. P. Feynman, *et al. J. Appl. Phys.* **28**, 49 (1957).

The direction of the Bloch vector can be specified either in Cartesian coordinates (x, y, z) or spherical polar coordinates (r, θ, φ), with

$$\begin{aligned} x &= r\sin\theta\cos\varphi, \\ y &= r\sin\theta\sin\varphi, \\ z &= r\cos\theta, \end{aligned} \tag{9.61}$$

as illustrated in Fig. 9.9. The requirement that the vector has unit length is satisfied when

$$r^2 = (x^2 + y^2 + z^2) = 1. \tag{9.62}$$

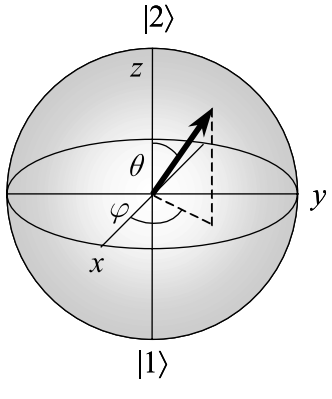

Fig. 9.9 The Bloch sphere. Coherent superposition states lie on the surface of the sphere, with their state defined by the angles (θ, φ) through eqn 9.64.

We therefore need only two independent variables to define an arbitrary state on the Bloch sphere, for example the angles (θ, φ). This allows us to make a unique mapping between the wave function amplitudes (c_1, c_2) and the direction of the Bloch vector.

The connection between the Bloch vector and the wave function may be made by defining the bottom and top of the sphere to correspond to the $|1\rangle$ and $|2\rangle$ states respectively, as shown in Fig. 9.9. The ground state with $|\psi\rangle = |1\rangle$ thus corresponds to $(0, 0, -1)$ in Cartesian coordinates or $\theta = \pi$ in polar coordinates. Similarly, the pure excited state $|2\rangle$

The choice of assigning the north and south poles of the Bloch sphere, respectively, to the upper and lower level is arbitrary. The analysis works equally well the other way round.

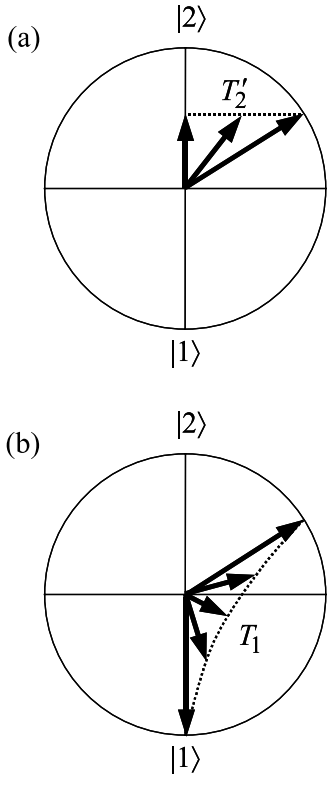

Fig. 9.10 Damping processes in the Bloch representation: (a) transverse (T_2') and (b) longitudinal (T_1) relaxation. T_2' processes conserve z but T_1 processes do not. In part (a) we are assuming that $T_2' \ll T_1$. Slower T_1 processes will eventually cause the excited state population to decay and the Bloch vector to return to the ground state with $\theta = \pi$. Note that the Bloch vector of the relaxed state is only meaningful for the entire ensemble rather than for individual atoms. Note also that longitudinal decay inevitably causes transverse relaxation as well.

corresponds to the point $(0, 0, 1)$ or $\theta = 0$. An arbitrary state is given in Cartesian coordinates as:

$$\begin{aligned} x &= 2\,\mathrm{Re}\langle c_1 c_2\rangle, \\ y &= 2\,\mathrm{Im}\langle c_1 c_2\rangle, \\ z &= |c_2|^2 - |c_1|^2. \end{aligned} \tag{9.63}$$

In polar coordinates this simplifies to (see Exercise 9.9):

$$\begin{aligned} c_1 &= \sin(\theta/2), \\ c_2 &= \mathrm{e}^{\mathrm{i}\varphi}\cos(\theta/2). \end{aligned} \tag{9.64}$$

This one-to-one mapping allows us to visualize an arbitrary superposition state of a two-level atom in a geometric way, which is very useful when considering the resonant interaction with an intense optical field.

It is instructive to compare superposition states with statistical mixtures in the Bloch representation. It is apparent that we can apply the Bloch model to individual atoms for the case of superposition states, but not for statistical mixtures. In the latter case the individual atoms are either in level 1 or in level 2, and it is only meaningful to calculate the Bloch vector for the whole ensemble. Furthermore, in a statistical mixture we have $\langle c_1 c_2\rangle = 0$ for every atom, which implies from eqn 9.63 that $x = y = 0$. Statistical mixtures thus correspond to points *inside* the Bloch sphere on the z-axis. Apart from the ground state with $|c_1|^2 = 1$, statistical mixtures therefore have $r < 1$, in contrast to superposition states, which are always on the surface of the sphere with $r = 1$.

In Section 9.5.2 we discussed the damping processes which destroy coherence and reduce superposition states to statistical mixtures. Since statistical mixtures have $r < 1$, damping processes do not conserve the modulus of the Bloch vector. Figure 9.10 illustrates the two different types of damping that can occur. Figure 9.10(a) illustrates the effect of damping by pure dephasing (T_2') processes. Such processes break the coherence without altering the populations, and they therefore correspond to scattering from the surface of the sphere towards the centre at constant z (cf. eqn 9.63). Figure 9.10(b) illustrates the contrasting effect of damping by population decay (T_1) processes. Since these affect the relative populations, they alter z as well.

The fact that pure dephasing (T_2') processes conserve z whereas population decay (T_1) processes do not explains why they are called transverse and longitudinal relaxation, respectively. Note, however, that Fig. 9.10(b) clearly illustrates the point that longitudinal relaxation simultaneously produces transverse relaxation, even in the absence of pure dephasing processes. This is why the total dephasing rate in eqn 9.54 contains contributions from both pure dephasing and population decay processes.

Up to this point we have been neglecting the explicit time dependence of the wave functions. The two-level atom has an intrinsic angular frequency of ω_0, and in making the transformation to the Bloch representation, we find that the Bloch vector rotates at a constant angular

frequency of ω_0 around the z-axis. It is therefore convenient to make a coordinate transformation to a rotating frame so that the Bloch vector is stationary.

Let us now consider the interaction of the Bloch vector with resonant optical pulses at angular frequency ω. As demonstrated in eqn 9.33, the light field produces interaction terms at frequencies of $(\omega - \omega_0)$ and $(\omega + \omega_0)$. In the rotating frame, the term at $(\omega - \omega_0)$ causes a slow precession of the Bloch vector at the difference frequency, and is stationary at exact resonance. By contrast, the term at $(\omega + \omega_0)$ causes a very rapid precession at $\sim 2\omega_0$, and can be neglected because of its highly non-resonant nature. This is why we described the neglect of the terms at $(\omega + \omega_0)$ as the 'rotating wave approximation'.

The application of a short resonant pulse can be considered as a **coherent operation** on the Bloch vector. If the pulse duration is shorter than the damping time, the coherence of the wave function will be retained and the modulus of the Bloch vector conserved. Hence the pulse will only change the direction of the Bloch vector without altering its length. This means that the pulse acts as a **rotation operator**. We showed previously that a π-pulse can convert a system in the ground state $|1\rangle$ to the excited state $|2\rangle$, and vice versa. This corresponds to a change of θ by π radians, and explains the origin of the name 'π-pulse'. In general, it can be shown that the rotation angle is equal to the pulse area defined in eqn 9.51. Hence a $\pi/2$-pulse causes a rotation of $\pi/2$ radians, while a 2π-pulse causes a rotation of 2π radians, leaving the system unchanged. The Bloch vector can thus be manipulated at will by a sequence of resonant pulses of well-defined amplitude and relative phase.

Let us consider the effect of a sequence of exactly resonant pulses at angular frequency ω_0 on a system that is in the ground state at $t = 0$. The azimuthal angles of the Bloch sphere are initially undefined, which means that the choice of the axis of rotation for the first pulse is arbitrary. It is therefore convenient to choose the x and y-axis directions in such a way that the first pulse produces a rotation about, say, the y-axis, leaving the Bloch vector somewhere in x-z plane at the end of the pulse. The axis about which subsequent rotations take place is then determined by the phase of the pulse relative to the first one. For example, a pulse with a phase difference of 90° relative to the first one would rotate the Bloch vector about an axis at 90° to the first one: that is, the $-x$ axis. Combinations of pulses of the appropriate area and phase can then be used to move the Bloch vector to any particular point on the Bloch sphere. Figure 9.11 illustrates how an initial pulse with an area of $3\pi/4$ followed by a $\pi/2$-pulse with a relative phase of $-90°$ moves the system from the ground state to a point within the x-y plane with an azimuthal angle of $\pi/4$.

Coherent operations on the Bloch vector have been used for many years for quantum state preparation in NMR systems. They have also been used extensively in two-level atomic systems at optical frequencies for the description of coherent phenomena such as **photon echoes** and

See, for example, Mandel and Wolf (1995, Chapter 15). The rotating frame transformation is entirely analogous to the one described in Section E.2 for the treatment of Larmor precession in NMR.

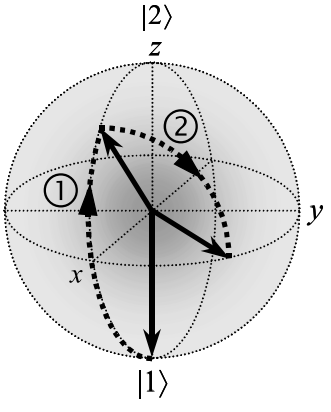

Fig. 9.11 The Bloch vector can be moved to arbitrary positions on the Bloch sphere by appropriate combinations of rotations. This figure illustrates the effect of a rotation by $3\pi/4$ about the y-axis followed by a rotation of $\pi/2$ about the x-axis on a Bloch vector initially in the ground state.

superradiance. In recent years the subject has acquired new importance in the practical implementation of quantum computation, both in NMR systems and also in the atomic systems at optical frequencies. This point will be developed further in Section 13.3.4 of Chapter 13.

Example 9.3 A pulsed laser beam is focussed to a spot of radius 1 μm on a gas of atoms with a dipole moment of 10^{-29} C m at the laser frequency.

(a) Calculate the pulse energy required to rotate the Bloch vector by $\pi/2$ radians for Gaussian pulses with a duration (FWHM) of 1 ps.

(b) If the system is initially in the ground state, find the state of the system at the end of the pulse.

Solution

(a) The time dependence of the electric field and intensity in a Gaussian pulse are given, respectively, by:

$$\mathcal{E}_0(t) = \mathcal{E}_{\text{peak}} \exp(-t^2/\tau^2),$$
$$I(t) = I_0 \exp(-2t^2/\tau^2). \tag{9.65}$$

We can relate τ to the pulse width by finding the time for the intensity to drop to half its peak value:

$$I(t_{1/2})/I_0 = \exp(-2t_{1/2}^2/\tau^2) = 0.5,$$

which implies $t_{1/2} = \sqrt{\ln 2/2}\tau$. Hence:

$$\tau_{\text{FWHM}} = 2t_{1/2} = 2\sqrt{\ln 2/2}\tau = 1.177\tau.$$

In our example we therefore find $\tau = 0.85$ ps.
The pulse energy E_{pulse} is related to the intensity by:

$$E_{\text{pulse}} = A \int_{-\infty}^{+\infty} I(t)\,\mathrm{d}t,$$

where A is the beam area. On making use of eqn 9.52 with Gaussian pulses and refractive index $n = 1$ we find:

$$\begin{aligned} E_{\text{pulse}} &= \frac{1}{2} Ac\epsilon_0 \int_{-\infty}^{+\infty} \mathcal{E}_0(t)^2\,\mathrm{d}t \\ &= \frac{1}{2} Ac\epsilon_0 \mathcal{E}_{\text{peak}}^2 \int_{-\infty}^{+\infty} \exp(-2t^2/\tau^2)\,\mathrm{d}t \\ &= \sqrt{\frac{\pi}{8}} Ac\epsilon_0 \mathcal{E}_{\text{peak}}^2 \tau. \end{aligned} \tag{9.66}$$

On the other hand, the pulse area Θ is given from eqn 9.51 by:

$$\begin{aligned} \Theta &= \frac{\mu_{12}}{\hbar} \int_{-\infty}^{+\infty} \mathcal{E}_0(t)\,\mathrm{d}t \\ &= \frac{\mu_{12}}{\hbar} \mathcal{E}_{\text{peak}} \int_{-\infty}^{+\infty} \exp(-t^2/\tau^2)\,\mathrm{d}t \\ &= \sqrt{\pi}\mu_{12}\mathcal{E}_{\text{peak}}\tau/\hbar. \end{aligned}$$

Thus for $\Theta = \pi/2$, $\mu_{12} = 10^{-29}$ C m and $\tau = 0.85$ ps we find $\mathcal{E}_{\text{peak}} = 11$ MV m^{-1}. On inserting into eqn 9.66 with $A = \pi(10^{-6})^2 = 3.1 \times 10^{-12}$ m^2, we finally find $E_{\text{pulse}} = 0.53$ pJ.

(b) The azimuthal angle for the rotation is arbitrary and so we choose to rotate within the $\varphi = 0$ plane. The state vector initially points downwards with $\theta = \pi$, and after the $\pi/2$-pulse we arrive at the point with $(\theta, \varphi) = (\pi/2, 0)$. We then find from eqn 9.64 that $c_1 = \sin(\pi/4) = 1/\sqrt{2}$ and $c_2 = \cos(\pi/4) = 1/\sqrt{2}$. Hence the final state of the system is:

$$|\psi\rangle = \frac{1}{\sqrt{2}}|1\rangle + \frac{1}{\sqrt{2}}|2\rangle = \frac{1}{\sqrt{2}}(|1\rangle + |2\rangle).$$

Further reading

The classic text on the theory of two-level atoms is Allen and Eberly (1975). The subject material of the chapter is covered in greater depth in the more advanced quantum optics texts such as Loudon (2000) or Mandel and Wolf (1995), while Foot (2005) covers the topics at a similar level from the perspective of atomic physics. Discussions of coherent phenomena such as photon echoes and superradiance may be found in nonlinear optics texts such as Yariv (1989) or Shen (1984).

Exercises

(9.1) The interaction between an atom and a light wave of angular frequency ω may be modelled classically as a driven oscillator system. The displacement of an electron in the atom by a distance x induces a dipole equal to $-ex$. The displacements have their own natural angular frequency ω_0, which is presumed to correspond to the transition frequency. The electric field of the light applies a force to the dipoles, and induces oscillations at its own frequency. The equation of motion for the displacement x of the electron is thus:

$$m_{\text{e}}\frac{\mathrm{d}^2x}{\mathrm{d}t^2} + m_{\text{e}}\gamma\frac{\mathrm{d}x}{\mathrm{d}t} + m_{\text{e}}\omega_0^2 x = F_0 \cos\omega t,$$

where m_{e} is the electron mass, γ is a damping constant, and F_0 is the amplitude of the force applied to the electron by the light. With the assumption that $\omega_0 \gg \gamma$, show that the magnitude of the driven oscillations is a maximum when $\omega = \omega_0$. What is the full width at half maximum of the resonance in angular frequency units?

(9.2) Write down the density matrix for the following superposition states:

(a) $|2\rangle$,
(b) $(|1\rangle + |2\rangle)/\sqrt{2}$,
(c) $(1/\sqrt{3})|1\rangle + (\sqrt{2/3})\mathrm{i}|2\rangle$.

(9.3) Write down the density matrix for a gas of two-level atoms at temperature T.

(9.4) The wave functions for hydrogenic states with quantum numbers (n, l, m_l) of (2,0,0) and (3,1,0) are as follows:

$$\psi_1(r,\theta,\varphi) = \frac{1}{4\sqrt{2\pi}{a_0}^{3/2}}\left(2 - \frac{r}{a_0}\right)\mathrm{e}^{-r/2a_0},$$
$$\psi_2(r,\theta,\varphi) = \frac{\sqrt{2}}{81\sqrt{\pi}a_0^{5/2}}\left(6 - \frac{r}{a_0}\right) r\cos\theta\,\mathrm{e}^{-r/3a_0}$$

where a_0 is the Bohr radius. Calculate the Einstein B coefficient B_{12}^{ω} for the 2s $\rightarrow$ 3p transition of atomic hydrogen for light polarized along the z-axis. Find also the Einstein A coefficient for the reverse transition.

(9.5) This exercise considers the case of Rabi oscillations when the light is not exactly resonant with the transition frequency. In the rotating wave approximation, eqn 9.33 becomes:

$$\dot{c}_1(t) = \frac{\mathrm{i}}{2}\Omega_\mathrm{R} \mathrm{e}^{\mathrm{i}\delta\omega t} c_2(t),$$
$$\dot{c}_2(t) = \frac{\mathrm{i}}{2}\Omega_\mathrm{R} \mathrm{e}^{-\mathrm{i}\delta\omega t} c_1(t),$$

where $\delta\omega = \omega - \omega_0$.

(a) Show that:

$$\ddot{c}_2 + \mathrm{i}\delta\omega\dot{c}_2 + (\Omega_\mathrm{R}^2/4)c_2 = 0.$$

(b) By considering a trial solution of the form $C\mathrm{e}^{-\mathrm{i}\zeta t}$, show that the general solution of this differential equation is:

$$c_2(t) = C_+ \mathrm{e}^{-\mathrm{i}\zeta_+ t} + C_- \mathrm{e}^{-\mathrm{i}\zeta_- t},$$

where $\zeta_\pm = (\delta\omega \pm \Omega)/2$, $\Omega^2 = \delta\omega^2 + \Omega_\mathrm{R}^2$, and C_+ and C_- are constants.

(c) Hence show that the initial conditions of $c_1(0) = 1$ and $c_2(0) = 0$ imply that:

$$|c_2(t)|^2 = \frac{\Omega_\mathrm{R}^2}{\Omega^2} \sin^2(\Omega t/2).$$

(9.6) In this exercise we investigate the behaviour of an ideal two-level atom with Einstein coefficients A_{21} and B_{12}^ω in the presence of a strong resonant field from a narrow bandwidth laser of angular frequency ω. The traditional Einstein analysis discussed in Section 4.1 assumes a broad-band radiation source and a narrow transition line, and therefore has to be modified to account for the situation that we are considering here, namely a narrow bandwidth radiation source.

We assume that the transition probability is proportional to the spectral line shape function $g_\omega(\omega')$, so that the frequency dependence of the absorption and stimulated emission rates are given, respectively, by:

$$W_{12}(\omega')\,\mathrm{d}\omega' = N_1 B_{12}^\omega u(\omega') g_\omega(\omega')\,\mathrm{d}\omega',$$
$$W_{21}(\omega')\,\mathrm{d}\omega' = N_2 B_{21}^\omega u(\omega') g_\omega(\omega')\,\mathrm{d}\omega',$$

where N_1 and N_2 are the populations of the lower and upper levels, and $u(\omega')$ is the energy density at frequency ω'.

(a) Consider first the case of a white broad-band source with a slowly varying energy density. Show that the transition rates written above are consistent with the traditional definitions of the Einstein coefficients.

(b) Now consider the case that we are interested in, namely that the spectral width of the laser is much smaller than the linewidth of the transition. Following Exercise (4.1), we write the spectral energy density as a delta function:

$$u(\omega') = u_\omega\, \delta(\omega' - \omega),$$

where u_ω is the energy density of the laser beam in $\mathrm{J\,m^{-3}}$. Show that the absorption and stimulated emission rates are now given, respectively, by:

$$W_{12} = N_1 B_{12}^\omega u_\omega g_\omega(\omega),$$
$$W_{21} = N_2 B_{21}^\omega u_\omega g_\omega(\omega).$$

(c) For simplicity, we now assume that the levels are non-degenerate, so that $B_{12}^\omega = B_{21}^\omega$ (see eqn 4.10). With the initial condition $N_2 = 0$, show that the time dependence of the fractional population of the upper level is given by:

$$\frac{N_2}{N_0} = \frac{B' u_\omega}{2B' u_\omega + A_{21}} \times \left[1 - \exp(-(2B' u_\omega + A_{21})t)\right],$$

where $B' = B_{12}^\omega g_\omega(\omega)$.

(d) Discuss the asymptotic behaviour for (1) very intense fields, and (2) weak fields.

(9.7) Referring to the data in Fig. 9.6(b), the transition dipole moment was 1.45×10^{-29} C m and the pulse duration (FWHM) was 7 ns. On the assumption that $n \approx 1$, estimate the maximum optical intensity in the pulse when the fluorescence intensity reaches its first maximum for the cases of: (a) a 'top hat' shaped pulse, and (b) a Gaussian pulse.

(9.8) Use the data in Fig. 9.7(a) to estimate the dipole moment of the optical transition in resonance with the laser beam. (Assume that $n \approx 1$.)

(9.9) Verify that eqn 9.64 is consistent with eqn 9.63.

(9.10) Find two-level superposition states that correspond to the following points on the Bloch sphere as defined by their polar angles (θ, φ):

(a) $(90°, 0)$,

(b) $(90°, 90°)$,

(c) $(90°, 180°)$,

(d) $(90°, -90°)$,

(e) $(60°, 45°)$.

(9.11) Find the points on the Bloch sphere corresponding to the following states, quoting your answer in Cartesian coordinates:

(a) $\psi = (\sqrt{1/3})|1\rangle + (\sqrt{2/3})|2\rangle$,

(b) $\psi = (\sqrt{2/3})|1\rangle - (\mathrm{i}/\sqrt{3})|2\rangle$,

(c) $\psi = (\mathrm{e}^{\mathrm{i}\pi/4}|1\rangle + |2\rangle)/\sqrt{2}$.

(9.12) Find the Bloch vector equivalent to an ensemble of two-level atoms with 60% of the atoms in the excited state and 40% in the ground state.

(9.13) A pulsed laser emits Gaussian pulses with a FWHM of 3 ps. The beam is focussed to a spot of radius 2 μm on a quantum dot with a dipole moment of 8×10^{-29} C m at the laser frequency. The refractive index of the crystal containing the quantum dot is 3.5.

(a) Calculate the pulse energy of a π-pulse.

(b) If the system is initially in the state $(1/\sqrt{2})(|1\rangle + |2\rangle)$, find the state of the system at the end of the pulse if its phase is set to rotate about the y-axis of the Bloch sphere.

(9.14) A two-level atom with a transition at angular frequency ω_0 and $\mu_{12} = 2 \times 10^{-29}$ C m is subjected to a sequence of two resonant pulses. The first pulse has an electric field given by $\mathcal{E}(t) = \mathcal{E}_1 \cos(\omega_0 t)$ and a duration of τ_1, while the second has $\mathcal{E}(t) = \mathcal{E}_2 \cos(\omega_0 t + \phi)$ and a duration of τ_2. $\mathcal{E}_1$ and $\mathcal{E}_2$ are both constant during the pulses, and the pulse length is much shorter than the dephasing time T_2. Given that the system starts in the ground state, find the final state when:

(a) $\mathcal{E}_1 = 4139$ V m,$^{-1}$ $\tau_1 = 1$ ns, $\mathcal{E}_2 = 6209$ V m^{-1}, $\tau_2 = 2$ ns, $\phi = 0$;

(b) $\mathcal{E}_1 = 827.8$ V m^{-1}, $\tau_1 = 10$ ns, $\mathcal{E}_2 = 3311$ V m^{-1}, $\tau_2 = 5$ ns, $\phi = 90°$;

(c) $\mathcal{E}_1 = 2.759 \times 10^4$ V m^{-1}, $\tau_1 = 0.3$ ns, $\mathcal{E}_2 = 5.519 \times 10^4$ V m^{-1}, $\tau_2 = 0.3$ ns, $\phi = 45°$.

10 Atoms in cavities

In the previous chapter we studied the resonant interaction between photons and an atomic transition of the same frequency. The atoms we considered were in free space and the photons originated from an external source such as a lamp or laser beam. We now wish to re-explore this process in more detail for the special case in which the interaction between the photons and the atom is enhanced by placing the atom inside a resonant cavity. This will naturally lead us into the subject of cavity quantum electrodynamics (cavity QED). We begin our discussion by considering the key parameters that determine the properties of the cavity and the magnitude of the atom–cavity coupling, and then explore the different physical effects that are observed in the limits of weak and strong coupling to the cavity.

10.1 Optical cavities

Before studying the interaction between atoms and cavities, it is helpful to remind ourselves of some of the basic properties of optical cavities. We shall restrict our attention here to the simplest case, namely a planar cavity. This will be sufficient to illustrate the chief points, and the results can then be generalized to other types of cavity. The planar cavity is covered in detail in most classical optics texts, and we give here only a brief summary of the results that are relevant to our discussion.

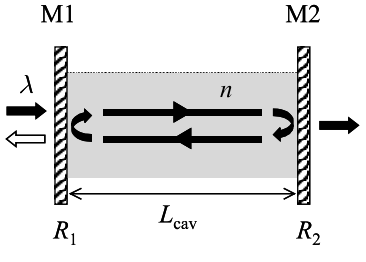

Fig. 10.1 A planar cavity of length $L_{\rm cav}$ with two parallel end mirrors M1 and M2 of reflectivity R_1 and R_2, respectively. The medium inside the cavity has a refractive index n. The cavity acts as a Fabry–Perot interferometer when light of wavelength λ is introduced through one of the end mirrors.

Consider the planar cavity shown in Fig. 10.1. The cavity consists of two plane mirrors M1 and M2, with reflectivities of R_1 and R_2, respectively, separated by an adjustable length $L_{\rm cav}$. The space between the mirrors is filled with a medium of refractive index n and the mirrors are aligned parallel to each other so that light inside the cavity bounces backwards and forwards between the mirrors. Planar cavities of the type shown in Fig. 10.1 are frequently used in high-resolution spectroscopy, in which case the instrument is called a **Fabry–Perot interferometer**.

The properties of the planar cavity can be analysed by considering the effect of introducing light of wavelength λ from one side and calculating how much gets transmitted through to the other side. On the assumption that there are no absorption or scattering losses within the cavity, the transmission $\mathcal{T}$ is given by:

$$\mathcal{T} = \frac{1}{1 + (4\mathcal{F}^2/\pi^2)\sin^2(\phi/2)} \tag{10.1}$$

See, for example, Brooker (2003), Hecht (2002), or Yariv (1997).

where

$$\phi = \frac{4\pi n L_{\rm cav}}{\lambda} \tag{10.2}$$

is the round-trip phase shift, and

$$\mathcal{F} = \frac{\pi (R_1 R_2)^{1/4}}{1 - \sqrt{R_1 R_2}} \tag{10.3}$$

is the **finesse** of the cavity. It is easy to see from eqn 10.1 that the transmission is equal to unity whenever $\phi = 2\pi m$, where m is an integer. In this situation the cavity is said to be **on-resonance**. From eqn 10.2 we see that the resonance condition occurs when the cavity length $L_{\rm cav}$ is equal to an integer number m of intracavity half wavelengths:

$$L_{\rm cav} = m\lambda/2n. \tag{10.4}$$

The resonance condition thus occurs when the light bouncing around the cavity is in phase during each round trip.

Figure 10.2 shows the transmission of a lossless planar cavity with $R_1 = R_2 = 0.9$, giving $\mathcal{F} = 30$. The transmission is a sharply peaked function of the round-trip phase shift ϕ, with maxima at the resonance values of $\phi = 2\pi m$. The width of the peaks can be calculated by finding the condition for $\mathcal{T} = 50\%$. In the limit of large $\mathcal{F}$, this is easily calculated from eqn 10.1 and gives

$$\phi = 2\pi m \pm \pi/\mathcal{F}. \tag{10.5}$$

The full width at half maximum (FWHM) is therefore equal to

$$\Delta\phi_{\rm FWHM} = 2\pi/\mathcal{F}, \tag{10.6}$$

which implies:

$$\mathcal{F} = \frac{2\pi}{\Delta\phi_{\rm FWHM}}. \tag{10.7}$$

The finesse of the cavity determines the resolving power when using the instrument for high-resolution spectroscopy.

The cavity resonance condition naturally leads to the concept of **resonant modes**. These are modes of the light field that satisfy the resonance condition and are preferentially selected by the cavity. Since the light fields bouncing around the cavity are all in phase, the waves interfere constructively and have much larger amplitudes than at non-resonant frequencies. The resonant modes have intensities inside the cavity enhanced by a factor $4/(1 - R)$ compared to an incoming wave, while the out of resonance frequencies have their intensity suppressed by a factor $(1 - R)$. (See Exercise 10.2.) The properties of the resonant modes play an essential part in determining the emission spectra of lasers, and will also be very important for the discussion of the emission properties of atoms in cavities.

The angular frequencies of the resonant modes are easily worked out from eqn 10.4 and are given by:

$$\omega_m = m\frac{\pi c}{n L_{\rm cav}}. \tag{10.8}$$

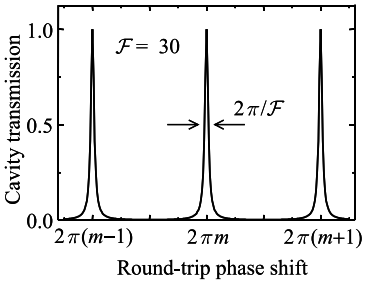

Fig. 10.2 Transmission of a lossless planar cavity with mirror reflectivities of 90%, giving a finesse $\mathcal{F}$ of 30. Resonance occurs whenever the round-trip phase equals $2\pi m$, where m is an integer.

The cavity finesse is usually defined as the ratio of the separation of adjacent maxima to the half width, as in eqn 10.7.

The cavity length is typically tuned by moving one of the mirrors with a piezoelectric transducer. The method used for tuning the refractive index depends on whether the cavity is filled with a gas or a solid. In the former case, the refractive index can be controlled through the gas pressure, and in the latter, by heating the cavity and using the temperature dependence of n.

The mode frequencies can be tuned either by changing $L_{\rm cav}$ or n. Since the mode frequency is proportional to the phase, we can use eqn 10.7 to relate the spectral width $\Delta\omega$ of the resonant modes to the properties of the cavity:

$$\frac{\Delta\omega}{\omega_m - \omega_{m-1}} = \frac{\Delta\phi_{\rm FWHM}}{2\pi} = \frac{1}{\mathcal{F}}, \tag{10.9}$$

giving:

$$\Delta\omega = \frac{\pi c}{n\mathcal{F}L_{\rm cav}}. \tag{10.10}$$

This shows that cavities with high finesse values have sharp resonant modes.

The final quantity that we need to consider is the **photon lifetime** $\tau_{\rm cav}$ inside the cavity. Consider a light source at the centre of a symmetric, high-finesse cavity with $R_1 = R_2 \equiv R \approx 1$. We suppose that the source emits a short pulse of light containing N photons into the cavity mode at time $t = 0$ as shown in Fig. 10.3. We assume that the fractional photon number change at each reflection is small due to the high reflectivity of the mirrors. After a time $t = nL_{\rm cav}/c$, the pulse will have gone around half the cavity, and the photon number will be equal to RN. At $t = 2nL_{\rm cav}/c$, the pulse will have completed a round trip and the photon number will be equal to R^2N. This process continues until all the photons are lost from the cavity. On average, we lose $\Delta N = (1 - R)N$ photons in a time equal to $nL_{\rm cav}/c$. We can therefore write:

$$\frac{{\rm d}N}{{\rm d}t} = -\frac{\Delta N}{nL_{\rm cav}/c} = -\frac{c(1-R)}{nL_{\rm cav}}N, \tag{10.11}$$

which has solution $N = N_0 \exp(-t/\tau_{\rm cav})$, where the photon lifetime is given by:

$$\tau_{\rm cav} = \frac{nL_{\rm cav}}{c(1-R)}. \tag{10.12}$$

It is helpful to define the **photon decay rate** (κ) as:

$$\kappa = \frac{1}{\tau_{\rm cav}}. \tag{10.13}$$

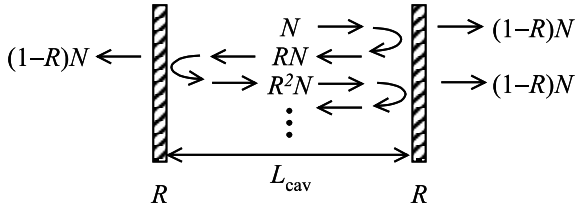

Fig. 10.3 Decay of the cavity photon number following emission from a pulsed source at the centre of the cavity at $t = 0$. The mirror reflectivities are assumed to be high, so that the fractional loss per round trip is small.

We can then combine eqns 10.3, 10.10, and 10.12 with $R \approx 1$ to find:

$$\Delta\omega = (\tau_{\rm cav})^{-1} \equiv \kappa. \tag{10.14}$$

This shows that the width of the resonant modes is controlled by the photon loss rate in the cavity, in exactly the same way that the natural width of an atomic emission line is controlled by the spontaneous emission rate (cf. eqn 4.30).

The analysis of the linear cavity shows that there are basically two key parameters that determine the main properties, namely the resonant mode frequency ω_m and the cavity finesse $\mathcal{F}$. The latter parameter controls both the mode width $\Delta\omega$ and the cavity loss rate κ. In dealing with other types of cavity it is helpful to introduce the **quality factor** (Q) of the cavity, defined by:

$$Q = \frac{\omega}{\Delta\omega}. \tag{10.15}$$

This serves the equivalent purpose for a general cavity as the finesse does for the planar cavity. It is thus convenient to specify the properties of a cavity either by the frequency and finesse, or equivalently by the frequency and quality factor.

10.2 Atom–cavity coupling

Having reminded ourselves of the relevant properties of optical cavities, we can now start to discuss the interaction between the light inside a cavity and an atom, as shown schematically in Fig. 10.4. We assume that the atom is inserted in such a way that it can absorb photons from the cavity modes and also emit photons into the cavity by radiative emission. We are particularly interested in the case where the transition frequency of the atom coincides with one of the resonant modes of the cavity. In these circumstances, we can expect that the interaction between the atom and the light field will be strongly affected, since the atom and cavity can exchange photons in a resonant way.

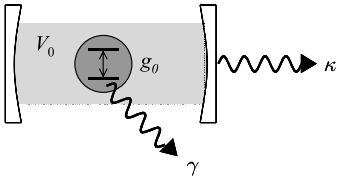

Fig. 10.4 A two-level atom in a resonant cavity with modal volume V_0. The cavity is described by three parameters: g_0, κ, and γ which, respectively quantify the atom–cavity coupling, the photon decay rate from the cavity, and the non-resonant decay rate. Note that the cavity in Fig. 10.4 is drawn with concave mirrors rather than plane ones. If the cavity only had plane mirrors, then off-axis photons emitted by the atom would never re-interact with it. The use of concave mirrors reduces this problem.

The transition frequencies of the atom are determined by its internal structure and are taken as fixed in this analysis. The resonance condition is then achieved by tuning the cavity so that the frequency of one of the cavity modes coincides with that of the transition. At resonance we find that the relative strength of the atom–cavity interaction is determined by three parameters:

- the photon decay rate of the cavity κ,
- the non-resonant decay rate γ,
- the atom–photon coupling parameter g_0.

These three parameters each define a characteristic time-scale for the dynamics of the atom–photon system. The interaction is said to be in the **strong coupling** limit when $g_0 \gg (\kappa, \gamma)$, where (κ, γ) represents the larger of κ and γ. Conversely, we have **weak coupling** when $g_0 \ll (\kappa, \gamma)$.

In the strong coupling limit, the atom–photon interaction is faster than the irreversible processes due to loss of photons out of the cavity mode. This makes the emission of the photon a *reversible* process in which the photon is re-absorbed by the atom before it is lost from the cavity. In the weak coupling limit, by contrast, the emission of the photon by the atom is an *irreversible* process, as in normal free-space spontaneous emission, but the emission rate is affected by the cavity. To proceed further we therefore need to consider the relative magnitudes of κ, γ, and g_0.

We start with the cavity photon decay rate κ. The photon decay rate was defined in eqn 10.13, and is governed by the properties of the cavity that determine its quality factor Q. This can be seen from eqns 10.14 and 10.15, which show that κ is related to Q by:

$$\kappa = \omega/Q. \tag{10.16}$$

Hence high Q values mean relatively small photon decay rates. In practice, very high Q factors are required before any of the interesting effects described in this chapter are observed.

The non-resonant decay rate γ is determined by several factors. The atom could emit a photon of the resonant frequency in a direction that does not coincide with the cavity mode, for example, sideways, as suggested by Fig. 10.4. Alternatively, the atom could decay to other levels, emitting a photon of a different frequency that is not in resonance with the cavity. Yet again, the atom in the excited state could be scattered to other states and perhaps decay without emission of a photon at all. The first of these processes is a property of the cavity. The second is determined by the internal dynamics of the atom, and represents a breakdown of the two-level atom approximation. The final process is connected with the same sort of scattering events that cause dephasing. (See Section 9.5.2.)

See Sections 9.5.2 and 9.6 for explanations of the terms 'transverse' and 'longitudinal' decay rates. The factor of two difference between the rates in eqn 10.17 comes from eqn 9.54 with the pure dephasing rate equal to zero, as appropriate for an isolated atom. The factor of $(1 - \Delta\Omega/4\pi)$ accounts for the fraction of the photons generated by spontaneous emission that are emitted at angles so that they are lost from the cavity.

For the case of radiative decay to non-resonant photon modes, we can set γ equal to the transverse dephasing rate:

$$\gamma \equiv 1/T_2 = \gamma_{\parallel}/2, \tag{10.17}$$

where $\gamma_{\parallel}$ is the longitudinal decay rate given by:

$$\gamma_{\parallel} = A_{21}(1 - \Delta\Omega/4\pi), \tag{10.18}$$

A_{21} being the Einstein A coefficient for spontaneous emission into free space, and $\Delta\Omega$ the solid angle subtended by the cavity mode.

This leaves us with the third parameter, namely the atom–cavity coupling rate g_0. In Chapter 9 we studied how two-level atoms interact with resonant light fields originating from external sources such as a lamp or laser. The situation we are considering here is slightly more complicated, because there is no external source to determine the field strength. We therefore have to consider the interaction between the atom and the vacuum field that exists in the cavity due to the zero-point fluctuations of the electromagnetic field. (See Section 7.4.)

The interaction energy ΔE between the atom and the cavity vacuum field is set by the electric dipole interaction (cf. eqn 9.25):

$$\Delta E = |\mu_{12}\mathcal{E}_{\rm vac}|, \tag{10.19}$$

where $\mu_{12} \equiv -e\langle 1|x|2\rangle$ is the electric dipole matrix element of the transition, and $\mathcal{E}_{\rm vac}$ is the magnitude of the vacuum field as given by eqn 7.37. On setting ΔE equal to $\hbar g_0$ we then find:

$$g_0 = \left(\frac{\mu_{12}^2\omega}{2\epsilon_0\hbar V_0}\right)^{1/2}. \tag{10.20}$$

It is therefore apparent that the atom–photon coupling rate is determined by the dipole moment μ_{12}, the angular frequency ω, and the modal volume V_0.

Equation 10.20 allows us to compare the atom–photon coupling rate directly with the dissipative loss rate, and hence determine whether we are in the strong or weak coupling regime, respectively. If we assume that the cavity loss rate κ is the dominant loss mechanism, we can use eqn 10.16 to see that strong coupling occurs when:

$$g_0 \gg \omega/Q. \tag{10.21}$$

We then find from eqn 10.20 that the condition for strong coupling is:

$$Q \gg \left(\frac{2\epsilon_0\hbar\omega V_0}{\mu_{12}^2}\right)^{1/2}. \tag{10.22}$$

We shall see in Example 10.1 below that this condition is very strict, and requires cavities with very high Q values. In most cases, single atom systems will therefore be in the weak coupling regime, especially when the loss rate to non-resonant modes is significant. The situation improves, however, if we have N atoms in the cavity. The criterion for strong coupling is then given by (cf. eqn 10.49 below):

$$\sqrt{N}g_0 \gg (\kappa, \gamma). \tag{10.23}$$

The factor of $\sqrt{N}$ makes it easier to observe strong coupling.

Example 10.1 An air-spaced symmetric planar cavity of length 60 μm and modal volume 5×10^{-14} m^3 is locked to resonance with a cesium transition at 852 nm which has $|\mu_{12}| = 3 \times 10^{-29}$ C m.

(a) Estimate the smallest values of the cavity Q, the cavity finesse, and the mirror reflectivity required for strong coupling for a single atom.

(b) The radiative lifetime of the transition is equal to 32 ns. Confirm that the atom–cavity coupling is larger than the non-resonant radiative loss rate.

The parameters in this example are based on the experiments described by W. Lange *et al.* in *Microcavities and Photonic Bandgaps*, Ed. J. Rarity and C. Weisbuch, Kluwer Academic Publishers, Dordrecht, 1996, pp. 443–56.

Solution

(a) For strong coupling we require $g_0 \gg \kappa$. We can substitute the values of V_0 and μ_{12} into eqn 10.20 with $\omega = 2\pi c/\lambda = 2.2 \times 10^{15}$ rad s^{-1} to

find $g_0 = 1.5 \times 10^8$ rad s^{-1} for this cavity. On using eqn 10.21, we then find $Q \gg 1.5 \times 10^7$. This value of Q implies from eqn 10.15 that the modal angular linewidth must be less than $g_0 = 1.5 \times 10^8$ rad s^{-1}. On substituting this value into eqn 10.10, we then find $\mathcal{F} \gg 1.1 \times 10^5$. Finally, with $\kappa \ll 1.5 \times 10^8$ s^{-1}, we find from eqns 10.12 and 10.13 that $(1-R) \ll 2.9 \times 10^{-5}$. Hence we require mirrors with reflectivities greater than 99.997%.

Although mirrors of such high reflectivities are not readily available, they can nonetheless be obtained from specialist optical coating companies.

(b) We first calculate the longitudinal decay rate from eqn 10.18. Since the length of the cavity is very much larger than the wavelength, we can assume that the solid angle subtended by the cavity mode is small. Hence we can put

$$\gamma_{\parallel} = A_{21} = 1/\tau_{\mathrm{R}} = 3.1 \times 10^7 \text{ s}^{-1}.$$

We then find the non-resonant decay rate from eqn 10.17, giving $\gamma = 1.6 \times 10^7$ s^{-1}. This is an order of magnitude smaller than g_0.

10.3 Weak coupling

10.3.1 Preliminary considerations

It is important to realize that many of the conclusions of Section 10.3 can be reached by the classical theory of electromagnetism. By treating the atom as an oscillating electric dipole, classical electrodynamics can derive a formula similar to eqn 10.28 for the emission rate into free space and can also explain why the presence of a cavity alters that rate. (See Further Reading.) Moreover, the idea of controlling a radiative transition rate by the environment occurs in other branches of physics, for example, extended X-ray absorption fine structure (EXAFS). On the other hand, most of the results that are presented in Section 10.4 are completely inexplicable in the classical picture, since they depend on the presence of the vacuum field.

In the previous section we saw that the coupling strength between the atom and the cavity can be classified as either strong or weak. In this section we shall investigate the weak coupling limit, leaving strong coupling until Section 10.4.

Weak coupling occurs when the atom–cavity coupling constant g_0 is smaller than the loss rate due to either leakage of photons from the cavity (κ) or decay to non-resonant modes (γ). This means that photons are lost from the atom–cavity system faster than the characteristic interaction time between the atom and the cavity. The emission of light by the atom in the cavity is therefore *irreversible*, just as for emission into free space.

Since the effect of the cavity is relatively small in the weak coupling limit, it is appropriate to treat the atom–cavity interaction by perturbation theory. In Section 10.3.2 we shall first use Fermi's golden rule to calculate the emission rate for the atom in free space, and then in Section 10.3.3 we shall calculate the revised rate when the atom is coupled resonantly to a single mode of a high-Q cavity. We shall see that the main effect of the cavity is to enhance or suppress the photon density of states compared to the free-space value, depending on whether the cavity mode is resonant with the atomic transition or not. This then either enhances or suppresses the radiative emission rate through the density of states factor that appears in Fermi's golden rule (see eqn 10.24 below). The spontaneous emission rate from an excited state of an atom is therefore not an absolute number, but can in fact be controlled by suppressing or enhancing the photon density of states by means of a resonant cavity.

10.3.2 Free-space spontaneous emission

The standard treatment of spontaneous emission based on Fermi's golden rule and the Einstein A coefficient is discussed in more detail in Section 4.2.

Before considering the spontaneous emission of an atom to a single resonant cavity mode, it is helpful to remind ourselves of the theory of dipole emission in free space. To do this, it is helpful to consider the properties of an emissive atom in a large cavity of volume V_0. This cavity is considered to be large enough that it has a negligible effect on the properties of the atom, and is merely incorporated to simplify the calculation.

The transition rate for spontaneous emission is given by Fermi's golden rule:

$$W = \frac{2\pi}{\hbar^2}|M_{12}|^2 g(\omega), \tag{10.24}$$

where M_{12} is the transition matrix element and $g(\omega)$ is the density of states. For the density of states we use the standard result for photon modes in free space (see eqn C.11 in Appendix C):

$$g(\omega) = \frac{\omega^2 V_0}{\pi^2 c^3}, \tag{10.25}$$

while for the matrix element we use the electric dipole interaction:

$$M_{12} = \langle \boldsymbol{p} \cdot \boldsymbol{\mathcal{E}} \rangle . \tag{10.26}$$

Since there is no external field source within the cavity, we must use the vacuum field for $\boldsymbol{\mathcal{E}}$. On substituting from eqn 7.37 and averaging over all possible orientations of the atomic dipole with respect to the field direction, we then obtain:

$$M_{12}^2 = \frac{1}{3}\mu_{12}^2 \mathcal{E}_{\mathrm{vac}}^2 = \frac{\mu_{12}^2 \hbar\omega}{6\epsilon_0 V_0}. \tag{10.27}$$

Hence from eqn 10.24 we find the final result:

$$W \equiv \frac{1}{\tau_{\mathrm{R}}} = \frac{\mu_{12}^2 \omega^3}{3\pi\epsilon_0 \hbar c^3}, \tag{10.28}$$

τ_{R} being the radiative lifetime. We thus conclude that the emission rate is proportional to the cube of the frequency and the square of the transition moment.

The result for the radiative emission rate can be related to the treatment based on the Einstein coefficients. (See Section 4.1.) The spontaneous emission rate is given by the Einstein A coefficient:

$$W = A_{21} = \frac{\hbar\omega^3}{\pi^2 c^3} B_{21}^{\omega}, \tag{10.29}$$

where B_{21}^{ω} is the Einstein B coefficient derived in Section 9.4. On substituting for B_{21}^{ω} from eqn 9.43, we obtain the same result as eqn 10.28.

10.3.3 Spontaneous emission in a single-mode cavity: the Purcell effect

We now come to the main task of this section: to calculate the spontaneous emission rate for a two-level atom coupled to a single-mode resonant cavity in the weak coupling limit. This problem was first considered by E. M. Purcell in 1946, and the resulting change to the emission properties of the atom is now frequently called the **Purcell effect**.

See E. M. Purcell, *Phys. Rev.* **69**, 681 (1946).

Consider an atom in a single-mode cavity of volume V_0 as shown in Fig. 10.5(a). By 'single-mode' we mean that there is only one resonant mode of the cavity that is close to the emission frequency of the atom. There will of course be other modes in the cavity, but we neglect them in this analysis because they are assumed to be far from resonance. In the weak coupling limit it is possible to use a perturbative approach similar to that for the atom in free space. The emission rate is then given by Fermi's Golden rule as in eqn 10.24.

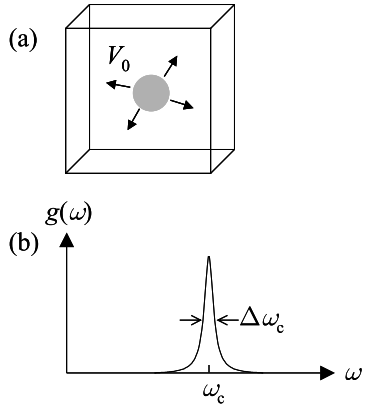

Fig. 10.5 (a) A two-level atom in a single-mode cavity with volume V_0. (b) Density of states function $g(\omega)$ for the cavity. The angular frequency of the cavity mode is ω_c, and $\Delta\omega_c$ is its linewidth.

We assume that the cavity mode has an angular frequency of ω_c with a half width $\Delta\omega_c$ determined by the quality factor Q. The density of states function $g(\omega)$ for the cavity will then take the form shown in Fig. 10.5(b). Since there is only one resonant mode, we must have:

$$\int_0^\infty g(\omega)\,\mathrm{d}\omega = 1, \tag{10.30}$$

which is satisfied if we use a normalized Lorentzian function for $g(\omega)$ (cf. eqn 4.29):

$$g(\omega) = \frac{2}{\pi\Delta\omega_c}\ \frac{\Delta\omega_c^2}{4(\omega-\omega_c)^2+\Delta\omega_c^2}. \tag{10.31}$$

If the frequency of the atomic transition is ω_0, then we must evaluate eqn 10.31 at ω_0 to obtain:

$$g(\omega_0) = \frac{2}{\pi\Delta\omega_c}\ \frac{\Delta\omega_c^2}{4(\omega_0-\omega_c)^2+\Delta\omega_c^2}. \tag{10.32}$$

At exact resonance between the atom and the cavity (i.e. $\omega_0 = \omega_c$), this reduces to:

$$g(\omega_0) = \frac{2}{\pi\Delta\omega_c} = \frac{2Q}{\pi\omega_0}, \tag{10.33}$$

where we have made use of eqn 10.15.

As with the free atom, we use the electric dipole matrix element given in eqn 10.26 and write in analogy to eqn 10.27:

$$M_{12}^2 = \xi^2\mu_{12}^2\mathcal{E}_{\mathrm{vac}}^2 = \xi^2\frac{\mu_{12}^2\hbar\omega}{2\epsilon_0 V_0}. \tag{10.34}$$

The factor ξ is the normalized dipole orientation factor defined by:

$$\xi = \frac{|\boldsymbol{p} \cdot \boldsymbol{\mathcal{E}}|}{|\boldsymbol{p}||\boldsymbol{\mathcal{E}}|}. \tag{10.35}$$

We can recall that ξ^2 averaged to 1/3 for the case of the randomly orientated dipole in free space.

On substituting eqns 10.32 and 10.34 into Fermi's golden rule (eqn 10.24), we obtain:

$$W^{\text{cav}} = \frac{2Q\mu_{12}^2}{\hbar\epsilon_0 V_0}\, \xi^2\, \frac{\Delta\omega_{\text{c}}^2}{4(\omega_0 - \omega_{\text{c}})^2 + \Delta\omega_{\text{c}}^2}, \tag{10.36}$$

where we have again made use of eqn 10.15. This rate can be compared to the free-space value given in eqn 10.28. We now introduce the **Purcell factor** F_{P} defined by:

$$F_{\text{P}} = \frac{W^{\text{cav}}}{W^{\text{free}}} \equiv \frac{\tau_{\text{R}}^{\text{free}}}{\tau_{\text{R}}^{\text{cav}}}. \tag{10.37}$$

On substituting from eqns 10.28 and 10.36 we then find:

$$F_{\text{P}} = \frac{3Q(\lambda/n)^3}{4\pi^2 V_0}\, \xi^2\, \frac{\Delta\omega_{\text{c}}^2}{4(\omega_0 - \omega_{\text{c}})^2 + \Delta\omega_{\text{c}}^2}, \tag{10.38}$$

where we have replaced c/ω by $(\lambda/n)/2\pi$, λ being the free-space wavelength of the light and n the refractive index of the medium inside the cavity. At exact resonance and with the dipoles orientated along the field direction, eqn 10.38 reduces to:

$$F_{\text{P}} = \frac{3Q(\lambda/n)^3}{4\pi^2 V_0}. \tag{10.39}$$

This is the main result of the analysis.

The Purcell factor is a convenient parameter that characterizes the effects of the cavity. Purcell factors greater than unity imply that the spontaneous emission rate is enhanced by the cavity, while $F_{\text{P}} < 1$ implies that the cavity inhibits the emission. Equation 10.39 shows that large Purcell factors require high Q cavities with small modal volumes. Furthermore, eqn 10.38 indicates that we need to have close matching between the cavity mode and the atomic transition, and we also need to ensure that the dipole is orientated as near to parallel with the mode field as possible. The enhancement of the emission rate on resonance is related to the relatively large density of states function at the cavity mode frequency. By contrast, the inhibition of emission when the atom is off-resonance is caused by the absence of photon modes into which the atom can emit.

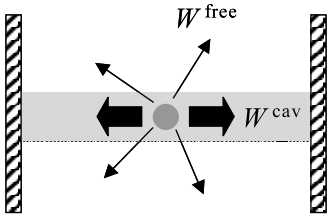

Fig. 10.6 An atom resonantly coupled to a planar cavity can emit both into the cavity mode and also to free-space modes.

Another useful parameter to describe the effects of the cavity is the **spontaneous emission coupling factor** β. This is the fraction of the number of photons emitted into the cavity mode to the total number of photons emitted. In an ideal cavity, the β-factor would be equal to unity. However, in a realistic cavity, there will still be emission into non-resonant modes and the β-factor will be less than unity.

Consider, for example, the scenario depicted in Fig. 10.6, which shows an atom resonantly coupled to a planar cavity. The atom will emit into the cavity mode at a rate W^{cav} given by eqn 10.36. However, since the direction of spontaneous emission is inherently random, it can also emit into free-space modes. The cavity only affects the density of states for modes in the direction along its axis, and it is therefore reasonable to assume that the density of free-space modes due to emission in all the other directions is largely unaffected by the cavity. If we write this emission rate into free-space modes as W^{free}, then the total emission rate will be equal to $(W^{\text{free}} + W^{\text{cav}})$. The β value is thus given by:

$$\beta = \frac{W^{\text{cav}}}{W^{\text{free}} + W^{\text{cav}}} = \frac{F_{\text{P}}}{1 + F_{\text{P}}}, \tag{10.40}$$

where we have made use of eqn 10.37. We thus conclude that the β-factor only approaches unity for large values of the Purcell factor.

This example is based on the experiments reported by Gérard *et al. Phys. Rev. Lett.* **81**, 1110 (1998) and discussed in Section 10.3.4 below.

Example 10.2 A semiconductor quantum dot emits at 900 nm and has a radiative lifetime of 1.3 ns. The dot is placed inside a GaAs microcavity of refractive index 3.5 with modal volume 1×10^{-19} m^{-3} and $Q = 2000$. Calculate the radiative lifetime in the cavity, on the assumption that the dipole moment is parallel to the mode field and that the cavity is exactly on resonance.

Solution

With the dipole parallel to the mode field, we have $\xi = 1$. Furthermore, at exact resonance we have $\omega_0 = \omega_c$. We can thus use eqn 10.39 to calculate the Purcell factor:

$$F_{\text{P}} = \frac{3 \times 2000 \times (9 \times 10^{-7}/3.5)^3}{4\pi^2 \times 10^{-19}} = 26.$$

We can then calculate the lifetime in the cavity using eqn 10.37:

$$\tau_{\text{R}}^{\text{cav}} = \frac{\tau_{\text{R}}^{\text{free}}}{F_{\text{P}}} = \frac{1.3 \text{ ns}}{26} = 0.05 \text{ ns}.$$

10.3.4 Experimental demonstrations of the Purcell effect

The first observations of the Purcell effect at optical frequencies were made in the late 1980s and early 1990s. See D. J. Heinzen *et al.*, *Phys. Rev. Lett.* **58**, 1320 (1987), F. De Martini *et al. Phys. Rev. Lett.* **59**, 2955 (1987), and A. M. Vredenberg *et al.*, *Phys. Rev. Lett.* **71**, 517 (1993). Observations at lower frequencies came earlier. See, for example, P. Goy *et al.*, *Phys. Rev. Lett.* **50**, 1903 (1983).

The observation of lifetime shortening by the Purcell effect at optical frequencies has posed a considerable challenge, since it ideally requires a very high Q cavity with a small modal volume. Some of the clearest observations in recent years have been made with semiconductor **microcavity** structures. These structures are primarily made to provide the wafers for vertical-cavity surface-emitting lasers (VCSELs) for

use in fibre optic systems. However, a spin-off of this technology has been the development of monolithic semiconductor structures with extremely small modal volumes ($V_0 \sim (\lambda/n)^3$) which demonstrate strong quantum optical effects. In this way it has been possible to use semiconductor microcavities to demonstrate both weak-coupling effects as discussed here, and also strong coupling: see Section 10.4.2 below.

Figure 10.7 shows a schematic diagram of a generic semiconductor microcavity. The entire structure is grown by techniques of semiconductor epitaxy. The active region usually contains quantum wells or quantum dots (see Appendix D), and the cavity is formed by two distributed Bragg reflector (DBR) mirrors. These mirrors are made by growing alternating layers of semiconductors with different refractive indices to form a highly reflecting quarter-wave stack. The active region is embedded within a spacer layer of thickness λ/n, λ being the vacuum emission wavelength of the active material and n the refractive index of the spacer material. In these conditions the planar cavity between the DBR mirrors supports a resonant mode with field antinodes at the mirrors and at the centre of the cavity. The materials chosen for the DBR mirrors and also the spacer region have larger band gaps than the active material, so that they are transparent at the wavelength of interest.

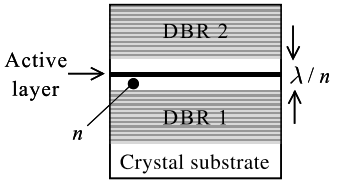

Fig. 10.7 A semiconductor microcavity. The structure consists of an active layer embedded within an inert spacer region of refractive index n, which is itself sandwiched between two DBR mirrors. The thickness of the spacer region is usually chosen to be equal to λ/n, where λ is the emission wavelength of the active material.

Note that the boundary conditions here are different from the usual case with field nodes at the mirrors. This occurs because of the similarity of the spacer region and the mirror materials.

Figure 10.8 shows results for the Purcell effect observed in InAs quantum dot micropillar structures at 8 K. Figure 10.8(a) gives a schematic diagram of the micropillar samples used for the experiment. The cylindrical micropillars were fabricated by reactive ion etching of a microcavity wafer grown by molecular beam epitaxy. The spacer region was made from GaAs, and the DBR mirrors were made from alternating layers of GaAs and AlAs. Both of these materials are transparent at the emission wavelength of the InAs quantum dots, namely 918 nm. The quantum dots were excited by 1.5 ps pulses at 838 nm from a mode-locked Ti : sapphire laser, and the photoluminescence was detected with a very fast detector called a streak camera.

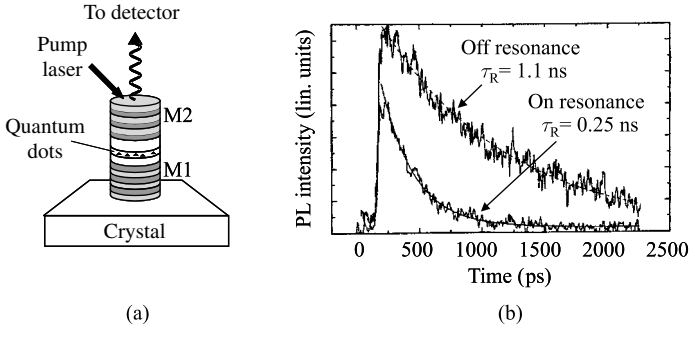

Fig. 10.8 (a) Schematic diagram of a quantum dot micropillar structure. (b) Photoluminescence (PL) decay curves measured for InAs quantum dot micropillar structures with a diameter of 1 μm at 8 K. The two curves compare the decays measured for on-resonance and off-resonance conditions. (After J. M. Gérard *et al.*, *Phys. Rev. Lett.*, **81**, 1110 (1998), ©American Physical Society, reproduced with permission.)

The results presented in Fig. 10.8(b) are for a micropillar with a diameter of 1 μm. The effective modal volume for this structure was estimated to be 1×10^{-19} m^{-3}, and the Q-factor was measured to be 2250, giving a Purcell factor from eqn 10.39 of 32. Two photoluminescence decay curves are shown corresponding to quantum dots of different frequencies that were either in resonance or far out of resonance with the cavity. The decay for the on-resonance dots is more than four times faster than that of the off-resonance dots, which clearly demonstrates the enhancing effect of the cavity. The difference between the measured lifetime reduction and the calculated Purcell factor is caused by inevitable variations in the crystal growth at the microscopic level. This produces an inhomogeneous distribution in the precise position and frequency of the quantum dots, making it impractical to detect the light coming exclusively from optimally coupled dots located exactly at the antinode of the cavity field.

10.4 Strong coupling

10.4.1 Cavity quantum electrodynamics

The conditions for strong coupling were described in Section 10.2. We require that the atom–cavity coupling rate g_0 shall be larger than the cavity decay rate set by the cavity lifetime and also the non-resonant atomic decay rate. In these conditions the interaction between the photons in the cavity mode and the atom is *reversible*. The atom emits a photon into the resonant mode, which then bounces between the mirrors and is re-absorbed by the atom faster than it is lost from the mode. The reversible interaction between the atom and the cavity field is thus faster than the irreversible processes due to loss of photons. This regime of reversible light–atom interactions is called **cavity quantum electrodynamics** (cavity QED).

See E. T. Jaynes and F. W. Cummings, *Proc. IEEE* **51**, 89 (1963).

The interaction between a resonant cavity mode and the atom was first analysed in detail by Jaynes and Cummings in 1963. The **Jaynes–Cummings model** describes the interaction of a two-level atom with a single quantized mode of the radiation field. The workings of the model are beyond the scope of this book and the reader is referred to the bibliography for further details. We summarize here the main conclusions.

We consider first the 'bare' states of an uncoupled resonant system with just a single atom of angular frequency ω in the cavity. The states are labelled by the state of the atom ψ and the number of photons n:

$$\Psi = |\psi; n\rangle. \tag{10.41}$$

The ground state corresponds to the state with the atom in the ground state and no photons in the cavity:

$$\Psi_0 = |g; 0\rangle. \tag{10.42}$$

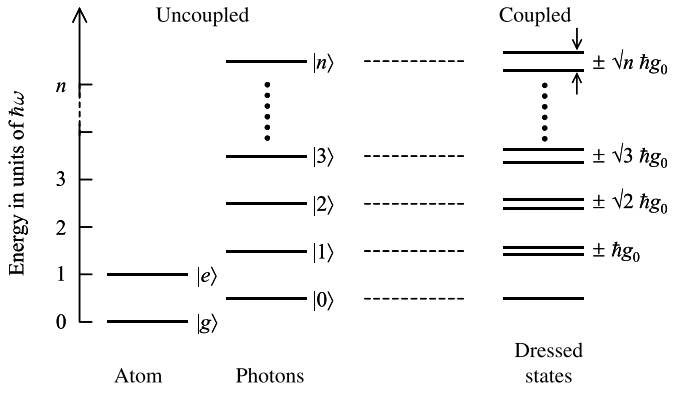

Fig. 10.9 The Jaynes–Cummings ladder. The ladder describes the states of a coupled atom–photon system with a coupling constant of g_0. The states of the uncoupled system are labelled by whether the atom is in the ground state $|g\rangle$ or the excited state $|e\rangle$, and by the number of photons n in the mode.

This has an energy of $(1/2)\hbar\omega$ due to the zero-point energy of the vacuum field in the cavity. The excited states are doubly degenerate. The first excited state is at energy $(3/2)\hbar\omega$, and corresponds to the states with either the atom in the excited state with no photons in the cavity $|e;0\rangle$ or the atom in the ground state with one photon in the cavity $|g;1\rangle$. Similarly, the nth excited state has energy of $(n+1/2)\hbar\omega$ and is derived from the states $|e;n-1\rangle$ and $|g;n\rangle$.

The effect of turning on the atom–cavity interaction is depicted in Fig. 10.9. The electric-dipole interaction between the atom and the photon mixes the degenerate states and lifts the degeneracy. The first excited state now consists of a doublet with energies given by:

$$E_1^{\pm} = (3/2)\hbar\omega \pm \hbar g_0, \tag{10.43}$$

and with corresponding wave functions:

$$\Psi_1^{\pm} = \frac{1}{\sqrt{2}}\left(|g;1\rangle \mp |e;0\rangle\right). \tag{10.44}$$

The nth level consists of a doublet with energies given by

$$E_n^{\pm} = (n+1/2)\hbar\omega \pm \sqrt{n}\hbar g_0, \tag{10.45}$$

and wave functions:

$$\Psi_n^{\pm} = \frac{1}{\sqrt{2}}\left(|g;n\rangle \mp |e;n-1\rangle\right). \tag{10.46}$$

Each level thus consists of a doublet with splitting:

$$\Delta E_n = 2\sqrt{n}\hbar g_0. \tag{10.47}$$

The mixed atom–photon states are called **dressed states**, and the ladder of doublets is called the **Jaynes–Cummings ladder**.

It is informative to compare the dressed states of the Jaynes–Cummings ladder to the dressed states discussed previously when considering Rabi flopping in Section 9.5. The Rabi model considers the resonant interaction between an atom and a *classical* field of high intensity, while the Jaynes–Cummings model considers the same phenomenon for quantized lights field with small photon numbers. Figure 10.9 can be

reconciled with Fig. 9.7(b) by equating the Rabi frequency in the latter with $2\sqrt{n}g_0$. The factor of two arises from difference between standing waves in a cavity and travelling waves from a laser beam, while the factor of $\sqrt{n}$ arises from the scaling of the energy ($\propto n$ for large n) with the square of the electric field amplitude. The splittings of the upper and lower levels in Fig. 9.7(b) are the same because we are considering adding or subtracting a photon to the field when n is already large and we can ignore the difference between $\sqrt{n}$ and $\sqrt{n \pm 1}$. The interesting point of the cavity system is that there is a splitting even for the first rung of the ladder. This splitting is called the **vacuum Rabi splitting**, and its magnitude is equal to (see eqn 10.20):

$$\Delta E^{\text{vac}} \equiv 2\hbar g_0 = \left(\frac{2\mu_{12}^2 \hbar \omega}{\epsilon_0 V_0} \right)^{1/2}. \tag{10.48}$$

The vacuum Rabi splitting can be understood as the AC Stark effect induced by the *vacuum* field.

The Jaynes–Cummings model can be adapted to the case of N atoms interacting with the single-mode field of a resonant cavity. In this case the vacuum Rabi splitting scales as the square root of N:

$$\Delta E^{\text{vac}}(N) = \sqrt{N}\Delta E^{\text{vac}} = \sqrt{N} \left(\frac{2\mu_{12}^2 \hbar \omega}{\epsilon_0 V_0} \right)^{1/2}. \tag{10.49}$$

If the medium within the cavity has a relative permittivity of ϵ_{r}, we should replace ϵ_0 with $\epsilon_{\text{r}}\epsilon_0 \equiv n^2\epsilon_0$, where n is the refractive index, to obtain:

$$\Delta E^{\text{vac}}(N) = \sqrt{N} \left(\frac{2\mu_{12}^2 \hbar \omega}{n^2 \epsilon_0 V_0} \right)^{1/2}. \tag{10.50}$$

These results are important for understanding the experimental results presented below. It is very challenging to observe the vacuum Rabi splitting from a single atom, and many experiments in fact measure the splitting for multi-atom systems.

The splitting of the modes of the atom–cavity system can be given a quasi-classical explanation by considering the properties of two coupled classical oscillators as shown in Fig. 10.10. If ω_1 and ω_2 are the natural angular frequencies of the uncoupled oscillators, (i.e. the cavity and atom,) and Ω is the coupling strength, then it can be shown that the frequencies of the coupled modes are given by

$$\omega_{\pm} = (\omega_1 + \omega_2)/2 \pm \left(\Omega^2 + (\omega_1 - \omega_2)^2\right)^{1/2}. \tag{10.51}$$

At resonance, with $\omega_1 = \omega_2 \equiv \omega$, this reduces to (see Exercise 10.9):

$$\omega_{\pm} = \omega \pm \Omega, \tag{10.52}$$

which can be compared to the Jaynes–Cummings result with $n = 1$ which gives essentially the same result. Of course, the classical model does not explain why there is a photon oscillator in the cavity in the

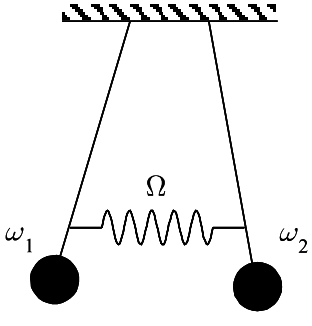

Fig. 10.10 Coupled oscillators. ω_1 and ω_2 are the natural frequencies of the uncoupled oscillators and Ω is the coupling strength.

first place: the vacuum field is a purely quantum effect with no classical analogue. However, if we take the vacuum field for granted, then the vacuum Rabi splitting can be understood as the frequency splitting of the normal modes of the coupled atom–cavity oscillators.

Example 10.3 A cavity of length 3.2 mm and modal volume 1.9×10^{-11} m^3 is tuned to resonance with one of the hyperfine lines of the sodium D_2 transition at 589 nm with $\mu_{12} = 2.1 \times 10^{-29}$ C m. Calculate the vacuum Rabi splitting frequency for a cavity containing 200 sodium atoms.

This example is based on the data presented in Fig. 10.11.

Solution
We first calculate the coupling parameter g_0 from eqn 10.20 for angular frequency $\omega_0 = 2\pi c/\lambda = 3.2 \times 10^{15}$ rad s^{-1}. This gives:

$$g_0 = \left(\frac{(2.1 \times 10^{-29})^2 (3.2 \times 10^{15})}{2\hbar\epsilon_0 (1.9 \times 10^{-11})} \right)^{1/2} = 6.3 \times 10^6 \text{ rad s}^{-1}.$$

Then from eqns 10.48 and 10.49 we find:

$$\Delta\Omega^{\text{vac}} = 2\sqrt{N} g_0 = 1.8 \times 10^8 \text{ rad s}^{-1}.$$

In an experiment we measure frequency rather than angular frequency, and we thus expect a vacuum Rabi splitting of 28 MHz.

10.4.2 Experimental observations of strong coupling

The observation of strong coupling requires cavities with small volumes to enhance the coupling constant g_0 and high Q-factors to reduce the photon loss rate. We also require that other dissipative rates due to dephasing and non-resonant emission should be minimized. Finally, we require that the cavity should support only a single mode in resonance with the atom. These requirements are very challenging, and it has taken many years to develop the techniques to achieve the goal of observing the vacuum Rabi splitting predicted by Jaynes–Cummings ladder.

Figure 10.11(a) shows a schematic diagram of an arrangement for observing the vacuum Rabi splitting in atomic physics. The apparatus consisted of a high-finesse resonant cavity through which a beam of sodium atoms was passed. A tunable probe laser was introduced through one of the mirrors and the intensity of the transmitted beam was measured with a detector. The resonant frequency of the cavity was locked to one of the hyperfine lines of the $3S_{1/2} \rightarrow 3P_{3/2}$ transition of the sodium atoms at 589.0 nm and the frequency of the probe laser was scanned through the resonant mode. The intensity of the probe laser was kept small so that the average photon number in the cavity was small. The finesse of the cavity was 26 000 and the cavity length was 3.2 mm. Although the cavity supported many modes, the finesse was sufficiently high that only one of them interacted strongly with the atomic transition.

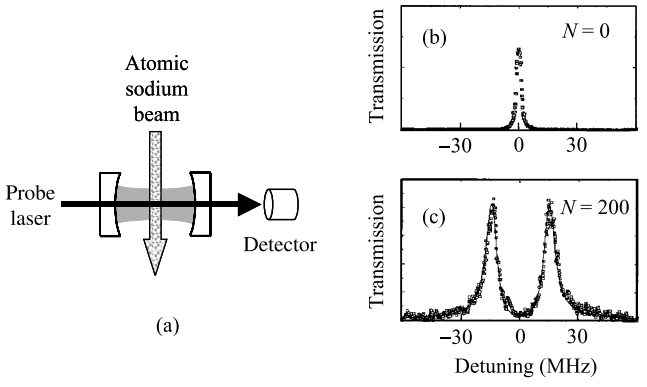

Fig. 10.11 Experimental demonstration of the vacuum Rabi splitting in atomic physics. (a) Experimental arrangement. (b) Transmitted intensity as a function of detuning from the resonant frequency with no atoms in the cavity. (c) Cavity transmission with the atomic beam turned on and the cavity locked to resonance with a transition at 589.0 nm. The average number N of atoms within the resonant mode was 200. (After H. J. Kimble in *Cavity quantum electrodynamics* (ed. P. R. Berman). Academic Press, San Diego, CA (1994), p. 203.)

The observation of the vacuum Rabi splitting for a *single* atom is reported in A. Boca *et al.*, *Phys. Rev. Lett.* **93**, 233603 (2004) and in P. Maunz *et al.*, *Phys. Rev. Lett.* **94**, 033002 (2005).

The results of the experiment are shown in Figs 10.11(b) and (c). Part (b) shows the transmission of the cavity when the atomic beam is switched off. In general, the cavity reflects the probe laser except when its frequency coincides with the resonant mode. We thus observe a single transmission peak at zero detuning. Part (c) shows the transmission with an average number of 200 atoms in the cavity. Two transmission peaks are now observed with their frequency shifted up and down from the empty-cavity value. The magnitude of the splitting was found to scale as the square root of the number of atoms, in agreement with eqn 10.49, and the absolute magnitude was in agreement with the experimental parameters of the cavity and the atoms. (See Example 10.3.) The results therefore clearly demonstrate strong coupling of the atoms to the cavity.

Strong coupling has also been observed in solid-state physics using semiconductor quantum well microcavities. The structures typically contain several semiconductor quantum wells embedded at the centre of the cavity formed between two mirrors as shown in Fig. 10.7. The whole structure is grown as a semiconductor wafer by techniques of advanced epitaxial crystal growth. The length of the cavity is generally chosen to match the wavelength of the strongest exciton line at the band edge of the quantum well. (See Fig. D.2.) Exact resonance is achieved by tuning the frequency of the exciton line to the fixed-length cavity by external parameters such as the temperature or electric field. Since the cavity is only one wavelength long, it supports just a single mode near the exciton line and we do not have to worry about other cavity modes. On the other hand, the presence of thermal excitations in the crystal causes rapid dephasing, and it is usually necessary to work at low temperatures to ensure that the atom–cavity coupling exceeds the broadening due to dephasing.

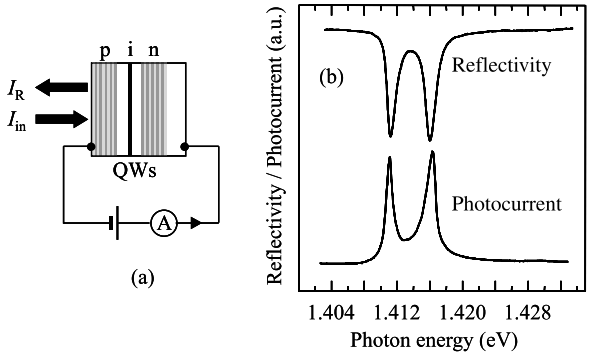

Fig. 10.12 (a) Experimental arrangement for reflectivity and photocurrent measurements on a GaAs/AlGaAs microcavity containing three InGaAs quantum wells (QWs). The top and bottom mirrors were p- and n-type doped respectively to form a p-n junction, with the quantum wells contained in a thin undoped intrinsic (i) region at the centre of the cavity, thus giving a p-i-n structure. $I_{\rm in}$ and $I_{\rm R}$ represent the incident and reflected light intensities, respectively. (b) Reflectivity and photocurrent spectra at 5 K. (After T. A. Fisher *et al.*, *Solid State Electronics* **40**, 493 (1996), © Elsevier, reproduced with permission.)

Figure 10.12 shows experimental data for a high Q microcavity containing three InGaAs/GaAs quantum wells. Tuning to exact resonance was achieved in this experiment by doping the mirrors to form a p-i-n structure as shown in part (a) of the figure. The quantum wells were undoped and were inserted within the depletion region of the junction, thereby experiencing a strong electric field when reverse bias was applied. Then by varying the bias voltage, the frequency of the exciton lines could be shifted to resonance by the Stark effect. The use of the p-i-n junction also permitted the measurement of the photocurrent generated after absorption of photons in the cavity.

Figure 10.12(b) shows the reflectivity and photocurrent spectra measured at resonance with $T = 5$ K. The reflectivity spectrum should show the opposite behaviour to the transmission, with high reflectivity when the cavity is off-resonance and a dip at the resonant frequency. This is observed when the cavity is out of resonance, but at resonance the mode splits into a doublet due to the vacuum Rabi splitting, as demonstrated in Fig. 10.12(b). The photocurrent spectrum gives a measure of the absorption strength within the cavity and shows complementary behaviour to the reflectivity. The fact that both lines generate a photocurrent demonstrates the mixed atomic–photon character of both components of the Rabi doublet.

Strong coupling has also been reported for *single* quantum dots in microresonator cavities at cryogenic temperatures. See J. P. Reithmaier *et al.*, *Nature* **432**, 197 (2004), T. Yoshie *et al.*, *Nature* **432**, 200 (2004), and E. Peter *et al.*, *Phys. Rev. Lett.* **95**, 067401 (2005).

10.5 Applications of cavity effects

The properties of atoms in cavities have found application in both the weak and strong coupling limits. We mention here two examples, one for

each type of coupling. Further examples may be found in the collections of papers cited in the bibliography.

Weak coupling microcavity techniques are routinely employed in VCSELs, which are now commonly employed in local area networks. The enhancement of the cavity reduces the lasing threshold and improves the directionality of the emission.

The most common application of cavity effects is in the production of low-threshold lasers. The idea is to employ the control of the spontaneous emission rate that can be achieved in a weakly coupled cavity to improve the performance of the laser medium. An interesting recent development of this basic idea is to employ **photonic crystals** to obtain better control of the spontaneous emission. A photonic crystal is a structure in which the dielectric properties are varied periodically on the length-scale of the wavelength of the light. When the light wavelength matches the period of the structure, Bragg reflection occurs and the light is unable to propagate. This creates a **photonic band gap**, which is analogous to the electronic band gaps formed in crystals when the electron wavelength matches the unit cell size.

The distributed Bragg reflector mirrors found in semiconductor microcavities have a periodic variation of the refractive index along the crystal growth direction, and are thus examples of one-dimensional photonic crystals. It is intuitively obvious that the effects of the cavity can be enhanced further by controlling the spontaneous emission in more than one direction. This requires a two- or three-dimensional periodic structure. The challenge of producing these engineered structures at optical wavelengths is the subject of much current research.

Natural photonic structures have recently been discovered in biology, notably in butterfly wings. See Vukusic and Sambles, *Nature* **424**, 852 (2003). The gemstone opal is another example of a natural photonic crystal.

The basic idea of the photonic crystal laser is shown schematically in Fig. 10.13. Figure 10.13(a) gives a schematic diagram of a two-dimensional photonic crystal containing a single emissive defect. The hexagonal pattern of black circles might typically represent holes etched into the surface of a semiconductor wafer, while the defect might be a quantum dot at the position where a hole would normally have been. The periodic structure prevents certain frequencies from propagating, and this creates a photonic band gap in the photon density of states as shown schematically in part (b) of the figure. The density of states

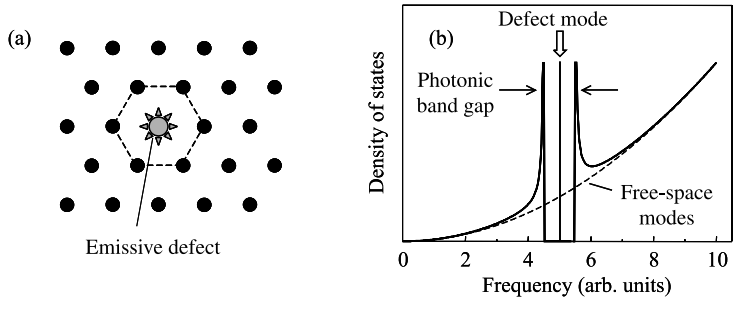

Fig. 10.13 (a) Schematic diagram of a two-dimensional photonic crystal with a hexagonal lattice containing a single emissive defect. The black circles represent air holes etched into the surface of the crystal. (b) Schematic density of states in a photonic crystal (solid) compared to free-space (dashed). The emission frequency of the defect mode is ideally chosen to be at the centre of the photonic band gap.

for free-space modes which follows an ω^2 dependence (cf. eqn 10.25) is shown for comparison.

In a perfect photonic crystal, the density of states drops to zero in the gap, and is enhanced at the edges. The defect creates a new state at the centre of the gap which has a large density of states compared to free space. If this mode coincides with the emission frequency of the defect, we expect enhanced emission properties. Alternatively, we can exploit the enhanced density of states at the edges of the band gap. Many researchers have now demonstrated low threshold lasers by these methods.

Details of a semiconductor laser operating on a two-dimensional photonic-band-gap defect mode may be found in Painter *et al.*, *Science* **284**, 1819 (1999), while Kopp *et al.* describe a dye-doped liquid crystal laser which exploits the enhanced density of states at the edges of a one-dimensional photonic band gap in *Opt. Lett.* **23**, 1707 (1998).

Turning now to the strong coupling phenomena, one of the most exciting applications is in the development of single-photon phase gates for use in quantum computation. The idea here is to create an atom–cavity system in which the addition of one atom or one photon produces a measurable alteration to the properties of the system. The key parameters are the **critical atom number** N_0 and **critical photon number** n_0, defined, respectively, by:

$$N_0 = 2\kappa\gamma/g_0^2$$
$$n_0 = 4\gamma^2/3g_0^2. \tag{10.53}$$

The observation of a single-photon phase gate requires $(n_0, N_0) \ll 1$. In these conditions the addition of a single photon makes a measurable difference to the system.

Figure 10.14 shows a schematic diagram of the experimental arrangement used to demonstrate a single-photon phase gate using cesium atoms. The apparatus comprises of an ultra-high-finesse cavity tuned to resonance with one of the atomic transitions of the cesium atom. The flux of the atomic beam was adjusted so that on average there was only ever one atom in the cavity at a time. The cavity was interrogated with two beams called the control and probe beams, respectively. The frequencies of these two beams were shifted slightly from each other to allow them to be distinguished experimentally. The experiment consisted in measuring the rotation of the polarization of the probe beam induced by a single photon in the control beam. Experimental rotation angles of around 15° were found conditional on the presence of the control beam. The importance of single-photon phase gates is that they can be used as conditional quantum logic gates in a quantum computer. This point is developed further in Chapter 13.

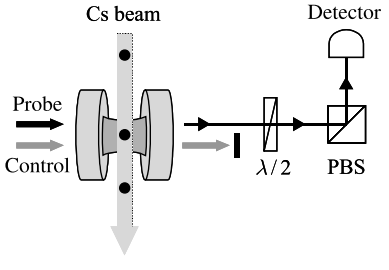

Fig. 10.14 Schematic diagram of a conditional phase gate using a single cesium atom. The polarization state of the transmitted probe beam was measured by using a half wave plate ($\lambda/2$) and a polarizing beam splitter (PBS). This enabled the polarization rotation angle induced by the control beam to be determined. (Adapted from Q. A. Turchette *et al.*, *Phys. Rev. Lett.* **75**, 4710 (1995).)

Further reading

The optical properties of planar cavities are considered in many optics texts, for example: Brooker (2003), Hecht (2002), or Yariv (1997).

A comprehensive collection of articles on cavity quantum electrodynamics can be found in Berman (1994). The chapter by Hinds in that

volume gives a very clear comparison of the classical and quantum-mechanical treatments of radiative emission in free space and cavities, while the chapter by Kimble gives a thorough review on work to observe strong coupling phenomena in atomic physics up to 1994. Rempe (1993) gives a more introductory treatment of the subject, while Kimble (1998) reviews work on single atom strong coupling. Vahala (2003) gives a clear overview of cavity effects in both atomic and solid state physics, while further details about experiments on quantum dots may be found in Michler (2003). A review of the present state-of-the-art for cavity QED experiments in atomic physics may be found in Miller *et al.* (2005).

The Jaynes–Cummings model is described in many theoretical quantum optics texts, for example: Gerry and Knight (2005), Meystre and Sargent (1999), or Yamamoto and Imamoglu (1999). A tutorial review may be found in Shore and Knight (1993).

Collections of review papers on atomic and solid state cavities, and also on photonic structures, may be found in Rarity and Weisbuch (1996) or Benisty *et al.* (1999). A tutorial review on confined electron and photon systems is given by Weisbuch *et al.* (2000), while more specific details about strong coupling in semiconductor microcavities are given by Skolnick *et al.* (1998).

Detailed treatments of photonic crystals made be found, for example, in Joannopoulos *et al.* (1995,1997) or Ozbay *et al.* (2004). Woldeyohannes and John (2003) give a tutorial review of the control of spontaneous emission in photonic materials.

Exercises

(10.1) Show that the quality factor of a planar cavity of finesse $\mathcal{F}$ is equal to $m\mathcal{F}$, where m is the mode number defined in eqn 10.8.

(10.2) By considering the field at an antinode, show that the optical intensity of a resonant mode inside a high-finesse symmetric cavity with mirror reflectivities of R is enhanced by a factor $4/(1-R)$ compared to the incoming intensity. Explain also why the average intensity within the cavity at off-resonant frequencies is diminished by a factor $(1-R)$.

(10.3) Calculate the photon lifetime for an air-spaced symmetric cavity with $R = 99\%$ and $L = 1$ mm.

(10.4) An air-spaced cavity designed for 589 nm has mirrors of reflectivity 99.9% and a length of 1 cm. Calculate the finesse and the Q-factor of the cavity.

(10.5) An air-spaced symmetric planar cavity of length 350 μm has a modal volume of 5×10^{-13} m^3. Estimate the smallest allowed values of (a) the cavity Q, (b) the cavity finesse, and (c) the mirror reflectivity to achieve strong coupling for a transition of a single cesium atom at 852 nm with $\mu_{12} = 3 \times 10^{-29}$ C m.

(10.6) Calculate the maximum mirror separation for a planar cavity that has just a single mode within the emission band of a fluorescent dye with peak emission at 600 nm and emission bandwidth of 40 nm. Assume that the cavity is filled with the dye and that the dye has a refractive index of 1.4.

(10.7) The semiconductor microcavity structures described in this chapter incorporate quarter-wave stack mirrors. (See Fig. 10.7.) Explain why a planar structure consisting of alternating layers of materials with refractive indices of n_1 and n_2 has a high reflectivity for light of air wavelength λ when the material thicknesses are chosen to be $\lambda/4n_1$ and $\lambda/4n_2$, respectively.

(10.8) A quantum dot emitting at 930 nm is placed at the centre of a resonant micropillar containing material of refractive index 3.5. The modal volume is 1.8×10^{-18} m^3 and the spectral width of the resonant mode is 0.18 nm. Calculate the Purcell factor.

(10.9) The equations of motion of two coupled classical oscillators of angular frequency ω may be written:

$$\ddot{x}_1 = -\omega^2 x_1 + 2\omega\Omega x_2,$$
$$\ddot{x}_2 = -\omega^2 x_2 + 2\omega\Omega x_1,$$

where x_1 and x_2 are the displacements of the oscillators, and Ω is the coupling frequency. Find the normal modes and frequencies of the coupled system, on the assumption $\Omega/\omega \ll 1$.

(10.10) Calculate the vacuum Rabi splitting frequency for the cavity in Exercise 10.5 with 100 atoms in the cavity mode.

(10.11) Consider the cavity described in Example 10.3, for which experimental data is presented in Fig. 10.11.

(a) Use the experimental data to estimate the photon lifetime for the cavity.

(b) Estimate the minimum number of atoms that have to be in the cavity to resolve the vacuum Rabi splitting, given that the radiative lifetime of the upper level is 16 ns.

(10.12) (a) The oscillator strength f_{ij} of an atomic transition $i \rightarrow j$ is defined by

$$f_{ij} = \frac{2m_0\omega_{ij}|\mu_{ij}|^2}{e^2\hbar}.$$

Use this definition to show that the vacuum Rabi splitting of a semiconductor microcavity of length $L_{\rm cav}$ containing $N_{\rm Q}$ quantum well layers at the centre of the cavity is given by:

$$\Delta E^{\rm vac} = \left(\frac{N_{\rm Q}e^2\hbar^2 f_{\rm area}}{\epsilon_0 m_0 n^2 L_{\rm cav}}\right)^{1/2},$$

where $f_{\rm area}$ is the oscillator strength per unit area of each quantum well layer and n is the refractive index of the semiconductor.

(b) Evaluate the vacuum Rabi splitting for a resonant microcavity of length 700 nm and refractive index 3.5 containing five quantum wells each with $f_{\rm area} = 6 \times 10^{16}$ m^{-2}.

(10.13) A cavity is made to the design of the cavity in Exercise 10.5 with a finesse that gives $\kappa/2\pi = 0.6$ MHz. Calculate the critical atom number and photon number for this cavity, given that the free-space radiative lifetime for the transition is 32 ns.